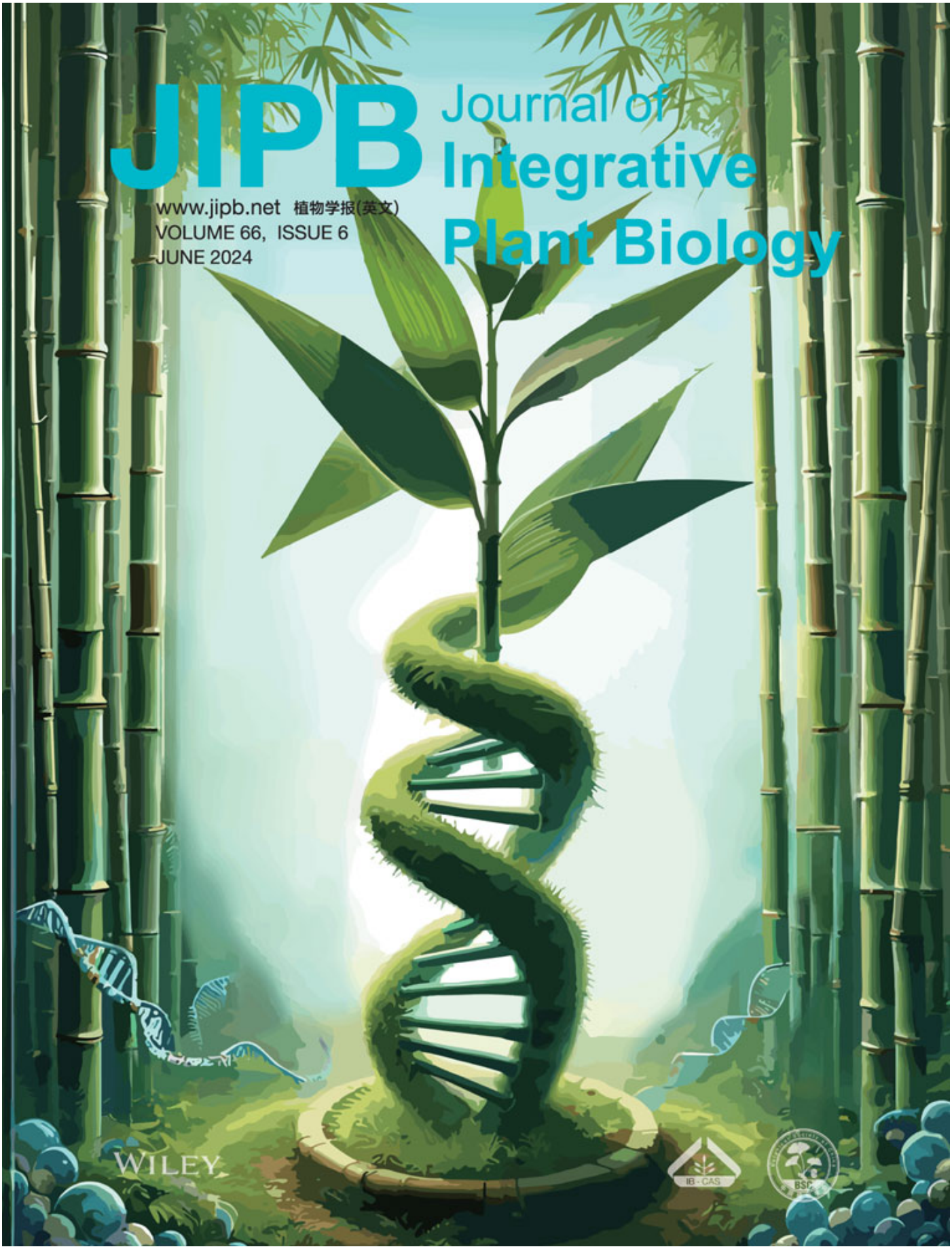
JIPB
Journal of
Integrative
Plant Biology
www.jipb.net 植物学报(英文)
VOLUME 66, ISSUE 6
JUNE 2024
WILEY
IB - CAS
BSP

JIPB Journal of Integrative Plant Biology

Research Article
https://doi.org/10.1111/jipb.13592

Chromosomal-level genome and metabolome analyses of highly heterozygous allohexaploid *Dendrocalamus brandisii* elucidate shoot quality and developmental characteristics[oo]

Jutang Jiang[1†], Zeyu Zhang[2†], Yucong Bai[1†], Xiaojing Wang[3], Yuping Dou[1], Ruiman Geng[1], Chongyang Wu[1], Hangxiao Zhang[2], Cunfu Lu[4], Lianfeng Gu[2*] and Jian Gao[1*]

1. Key Laboratory of National Forestry and Grassland Administration, Beijing for Bamboo & Rattan Science and Technology, Institute of Gene Science and Industrialization for Bamboo and Rattan Resources, International Center for Bamboo and Rattan, Beijing 100102, China
2. College of Forestry, Basic Forestry and Proteomics Research Center, Fujian Agriculture and Forestry University, Fuzhou 350002, China
3. School of Life Science, Peking University, Beijing 100871, China
4. College of Biological Sciences and Biotechnology, Beijing Forestry University, Beijing 100083, China

†These authors contributed equally to this work.

*Correspondences: Lianfeng Gu (lfgu@fafu.edu.cn); Jian Gao (gaojian@icbr.ac.cn, Dr. Gao is fully responsible for the distribution of the materials associated with this article)

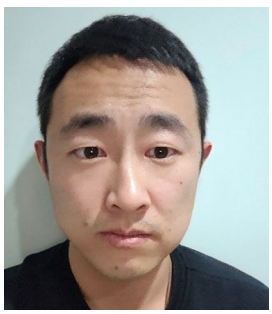

Jutang Jiang

Jian Gao

ABSTRACT

Dendrocalamus brandisii (Munro) Kurz is a sympodial bamboo species with inimitable taste and flavorful shoots. Its rapid growth and use as high-quality material make this bamboo species highly valued for both food processing and wood applications. However, genome information for *D. brandisii* is lacking, primarily due to its polyploidy and large genome size. Here, we assembled a high-quality genome for hexaploid *D. brandisii*, which comprises 70 chromosomes with a total size of 2,756 Mb, using long-read HiFi sequencing. Furthermore, we accurately separated the genome into its three constituent subgenomes. We used Oxford Nanopore Technologies long reads to construct a transcriptomic dataset covering 15 tissues for gene annotation to complement our genome assembly, revealing differential gene expression and post-transcriptional regulation. By integrating metabolome analysis, we unveiled that well-balanced lignin formation, as well as abundant flavonoid and fructose contents, contribute to the superior quality of *D. brandisii* shoots. Integrating genomic, transcriptomic, and metabolomic datasets provided a solid foundation for enhancing bamboo shoot quality and developing efficient gene-editing techniques. This study should facilitate research on *D. brandisii* and enhance its use as a food source and wood material by providing crucial genomic resources.

Keywords: bamboo shoots, *Dendrocalamus brandisii* (Munro) Kurz, flavonoid, genome, lignin

Jiang, J., Zhang, Z., Bai, Y., Wang, X., Dou, Y., Geng, R., Wu, C., Zhang, H., Lu, C., Gu, L., et al. (2024). Chromosomal-level genome and metabolome analyses of highly heterozygous allohexaploid *Dendrocalamus brandisii* elucidate shoot quality and developmental characteristics. J. Integr. Plant Biol. **66:** 1087–1105.

INTRODUCTION

Bamboo, a member of the Bambusoideae subfamily in the grass family (Gramineae), is one of the fastest-growing and most abundant forest resources. Bamboo species are broadly distributed in tropical and subtropical regions, playing a pivotal role in the economic advancement of numerous countries within these areas (Scurlock et al., 2000; Dixon and Gibson, 2014; Yang et al., 2018; Liu et al., 2020). In addition to its economic value, bamboo also holds significant ecological value, as its high carbon sequestration potential contributes to mitigating global climate change by acting as a carbon sink (Venkatachalam et al., 2015; Bhandawat et al., 2016). Based on the characteristics of their rhizomes, bamboos can be classified into three distinct groups: monopodial bamboos, sympodial bamboos, and mixed bamboos. Monopodial bamboos have a wide geographical distribution and spread rapidly, mainly growing in subtropical regions. Sympodial bamboos, which mainly grow in tropical regions, present a number of advantages over monopodial bamboos, including tall culms, high biomass production and carbon sequestration rate, and easy reproduction (Wang et al., 2010; Teng et al., 2016). To gain insight into the evolutionary characteristics and growth regulation mechanisms of bamboo, the genomes of four bamboo species with different geographical distributions have been sequenced. Additionally, chromosome-level whole-genome sequencing has been carried out for Moso bamboo (*Phyllostachys edulis*) and Ma bamboo (*Dendrocalamus latiflorus*). These efforts have greatly facilitated molecular mechanistic studies of related bamboo species (Peng et al., 2013; Zhao et al., 2018; Guo et al., 2019; Zheng et al., 2022).

Bamboo serves as a complete food source for certain animals and is valued as a health food and medicine for humans; its shoots are edible and are used for culinary purposes. Young bamboo shoots are consumed in various forms–fresh, dried, and fermented. Juvenile shoots not only have a delectable taste but are also highly nutritious, containing essential amino acids, carbohydrates, minerals, vitamins, and dietary fiber, while being low in fats and sugars. Moreover, shoots serve as an excellent source of health-enhancing bioactive compounds including phenols and phytosterols, contributing to the prevention of various diseases such as cancer, diabetes, and obesity (Chongtham et al., 2011b). In addition, bamboo shoots are an economically important source of timber. Over the last decade, remarkable progress has been achieved in exploring different aspects of bamboo shoot chemistry and biology. Based on spectroscopy analysis, bamboo shoots have been shown to contain substantial amounts of carbohydrates, amino acids, and nucleotides, as major chemical constituents (Sun et al., 2016). Additionally, metabolomic and phytochemical analyses have revealed the presence of L-phenylalanine, uridine, L-ornithine, L-tryptophan, and adenine, with L-phenylalanine contributing to the bitterness of bamboo shoots (Gao et al., 2019). The rapid growth of bamboo internodes in hedge bamboo (*Bambusa multiplex* (Lour.) Raeusch. Ex Schult) (Wei et al., 2019) and *P. edulis* (Chen et al., 2022) has been unveiled through a combination of morphological investigations and molecular biology assays. Bamboo shoot growth is regulated by phytohormones, including auxin (Li et al., 2018; Bai et al., 2023b) and cytokinins (Bai et al., 2023a). However, there has been a lack of sustained effort in consolidating the current knowledge regarding the fundamental nutritional aspects of bamboo shoots, as well as exploring more advanced facets of bamboo shoot biology. In addition, the current stage of bamboo genome sequencing and analysis of its shoot nutrient composition are not yet amenable to a comprehensive understanding of important biological characteristics such as bamboo shoot growth and palatability. An analysis of plastid genomes indicated that *Dendrocalamus brandisii* (Munro) Kurz (*D. brandisii*) is closely related to *D. latiflorus*, but these two species strongly differ in their shoot taste, with *D. brandisii* exhibiting superior shoot quality, even compared to *P. edulis* (He et al., 2020). Therefore, there is an urgent need to identify bamboos with excellent shoot characteristics in order to advance bamboo shoot research.

D. brandisii is a large tropical and subtropical evergreen sympodial bamboo species in the subfamily Bambusoideae (Gramineae). It originates from southern and northeastern India and Myanmar, and is mainly distributed in southern China, as well as in South and Southeast Asian countries, and Ethiopia, Bosnia, Herzegovina, and Brazil (Seethalakshmi et al., 1998; Zhan et al., 2018). *D. brandisii*, together with Hamilton's bamboo (*Dendrocalamus hamiltonii*) and giant bamboo (*Dendrocalamus asper*), are the three major sweet bamboo species in China, South Asia, and Southeast Asia. Their fresh shoots are of exceptional quality, possessing a sweet taste and containing the highest levels of glutamate and sugars among bamboo species used for shoot consumption in China. As a result, *D. brandisii* is one of the primary providers of high-quality edible shoots, satisfying both domestic demands and export needs (Li, 1997).

In addition to the excellent quality of its shoots, *D. brandisii* can regenerate shoots from callus (Lv et al., 2023), which serves as an important foundation for developing efficient gene-editing methodologies (Zhang and Wan, 2004; Zhong et al., 2019). Polyploid plants are generally larger and have higher nutrient contents compared to diploid plants. However, their genomes are also larger, posing challenges for genome sequencing. While the sequencing of polyploid genomes has been extensively conducted in crops, genome sequencing and assembly at the chromosome level in polyploid forest trees is rarely reported. A high-quality genome assembly for *D. brandisii* will pave the way for exploring bamboo shoot development. Here, we obtained a chromosome-level genome assembly for *D. brandisii* using PacBio single molecule real-time (SMRT) sequencing technology in conjunction with high-throughput chromosome conformation capture (Hi-C). Based on this sequence

information, we delineated three closely related subgenomes for *D. brandisii*. Additionally, we performed transcriptome sequencing of 15 different tissues using Oxford Nanopore Technology to help with genome annotation and to elucidate the factors determining the excellent quality and developmental pattern of *D. brandisii* shoots. The generation of a high-quality chromosome-level genome, extensive transcriptome data, and global metabolome data presented in this study not only provides valuable insights into the nutritional value of bamboo shoots but also greatly facilitates research on *D. brandisii*. Our data will serve as an important basis for studying bamboo shoot growth, development, and quality improvement.

RESULTS

Assembly of a high-quality, chromosome-scale *D. brandisii* genome

To investigate the molecular mechanism underlying *D. brandisii* growth and development, we assembled a high-fidelity genome for *D. brandisii* and performed gene annotation based on transcriptome data gathered by Nanopore sequencing from 15 tissues (Figure 1A). We initially constructed a genomic DNA library with an average insert size of 350 bp, which we sequenced on an Illumina instrument to perform a genome survey. This first analysis yielded a total of 206.15 Gb of high-quality data, corresponding to ~145× coverage. The results from GenomeScope analysis showed that the genome size of *D. brandisii* is approximately 1.42 Gb, with a GC content of around 45.0%. Heterozygosity was estimated at 2.65%, with a repetitive sequence content of about 61.85% (Figure S1). The *D. brandisii* genome thus exhibited characteristics of a complex and large genome with high heterozygosity and many repetitive elements.

To expand on this genomic survey, we employed circular consensus sequencing (HiFi) on a PacBio instrument, in combination with Hi-C reads to generate a full genome assembly for *D. brandisii*. After applying quality filters and data evaluation, we generated 144 Gb of clean data through HiC-Pro v2.10.0 analysis (Servant et al., 2015). We then employed LACHESIS (Burton et al., 2013) software to delineate, sort, and orient the genomic sequences into an oriented scaffold, followed by manual inspection. Following Hi-C correction and assembly, we obtained contig N50 values of 15,196,104 bp and scaffold N50 values of 38,763,808 bp. In total, we anchored 2,756,032,269 bp of allele-resolved genomic sequences onto 70 chromosomes, accounting for 98.0% of the genome, as estimated by short-read Illumina sequencing (Figure 1B). Furthermore, we divided the *D. brandisii* genome into subgenomes A (green), B (blue), and C (red) (Figure 1C), which provides the foundation for future analysis of subgenome evolution. We observed high syntenic blocks among the three subgenomes, which also shared syntenic blocks with the 12 chromosomes of the rice (*Oryza sativa*) genome.

Annotation of coding genes and repetitive sequences

To annotate the *D. brandisii* genome, we predicted all protein-coding genes by following three methodologies: homology-based prediction, *de novo* prediction, and transcriptome assembly. When combined, the outputs from the three approaches resulted in the identification of 126,817 genes (Figure 1B). Most of these genes were supported by at least two methods, reflecting the high quality of these predictions. We also evaluated the completeness of the resulting genome assembly by calculating the benchmarking of universal single-copy orthologs (BUSCO) score, which returned a score of 99.6% for our predicted genes, confirming a high level of genome completeness. We next annotated all predicted genes using the National Center for Biotechnology Information's (NCBI's) non-redundant (NR) database, eggNOG (Huerta-Cepas et al., 2019), Gene Ontology (GO), Kyoto Encyclopedia of Genes and Genomes (KEGG) (Kanehisa et al., 2016), SWISS-PROT (Boeckmann et al., 2003), and Pfam (Finn et al., 2006) databases. We succeeded in associating 95.6% of all genes with a functional annotation. We also identified 3,892 transfer RNA (tRNA) genes, 7,261 ribosomal RNA (rRNA) genes, and 666 microRNA loci using Infenal 1.1 (Nawrocki and Eddy, 2013).

The *D. brandisii* genome consists of 58.3% repetitive sequences, with transposable elements (TEs) accounting for 50.2%, and DNA transposons accounting for the remaining 8.1% (Figure 1B). Among the TEs, long terminal repeats (LTRs) were the most prominent, with 19.4% *Gypsy* and 18.7% *Copia* elements. Due to the repetitive nature of these elements, their assembly poses a significant challenge. To assess the quality of our genome assembly in the context of repetitive sequences, we estimated the continuity of LTR assembly by calculating the LTR Assembly Index (LAI), which falls into three categories: draft (LAI < 10), reference (10–20), and gold (LAI > 20) (Ou et al., 2018). The LAI for *D. brandisii* averaged 20.68, while most subgenomes having LAI values exceeding 20 (Figure 1C), indicating the high quality of our genome assembly.

Evolutionary analysis of the *D. brandisii* genome

In general, the size of bamboo genomes gradually increases from diploid herbaceous bamboos to tetraploid and hexaploid woody bamboos, with the insertion of TEs playing a major role in their genome expansion (Komatsuda et al., 2007). In the *D. brandisii* genome, the LTRs exhibited three recent bursts: approximately 0.046 million years ago (MYA), 1.092 MYA, and 1.475 MYA, similar to those observed for *D. latiflorus* (Figure 2A). However, herbaceous bamboo species experienced recent LTR bursts around 2–2.67 MYA, while tetraploid woody bamboos experienced bursts around 0.55–1.12 MYA. The LTRs bursts in hexaploid *D. brandisii* and *D. latiflorus* thus occurred much earlier, supporting their distinct evolutionary history. Notably, the most recent burst for *D. brandisii* was closer to that seen in maize (*Zea mays*) (Figure 2A).

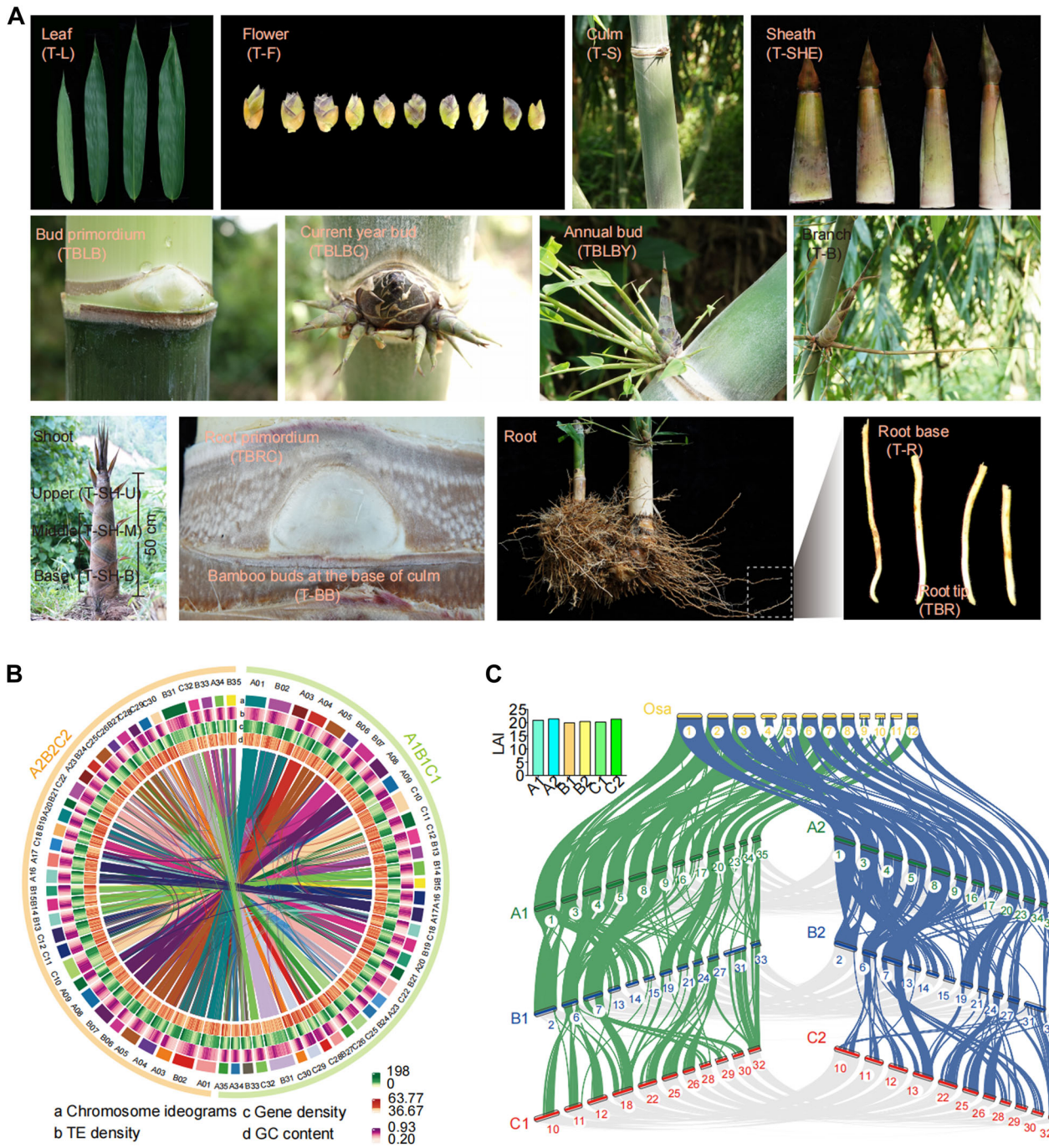

Figure 1. Chromosome-scale assembly of the *Dendrocalamus brandisii* genome

(A) Representative photographs of the tissue samples and the abbreviations used in this study for full-length transcriptome sequencing by Oxford Nanopore sequencing. The illustration in the bottom left corner incorporates three samples, representing the upper (T-SH-U), middle (T-SH-M), and lower base segments (T-SH-B) of the bamboo shoot. **(B)** Circos plot summarizing the genome features of the chromosome genome assembly produced for *D. brandisii* in this study. Concentric circles, from outer to inner circles, represent chromosomes (a), transposable element (TE) density (b), gene density (c), and GC content (d). A and B represent the two haplotypes. **(C)** Global collinearity relationships among *Oryza sativa* chromosomes and the three subgenomes of *D. brandisii*. The bar chart in the top left corner of the figure represents the Long terminal repeats Assembly Index (LAI) values of different subgenomes.

Using synonymous substitutions (Ks) and four-fold synonymous (degenerative) third-codon transversion (4DTv) analysis, we discovered that *D. brandisii* may have undergone two recent whole-genome duplication (WGD) events (Ks = 0.035 and 0.128), with values that are very similar to its closest relative *D. latiflorus* (Ks = 0.035 and 0.128) (Figure 2B, C). Notably, the paleotropical woody bamboo *B. amplexicaulis* only experienced the earliest WGD event (Ks = 0.137), while the temperate woody bamboo *P. edulis* only underwent one WGD event (Ks = 0.12). Therefore, based

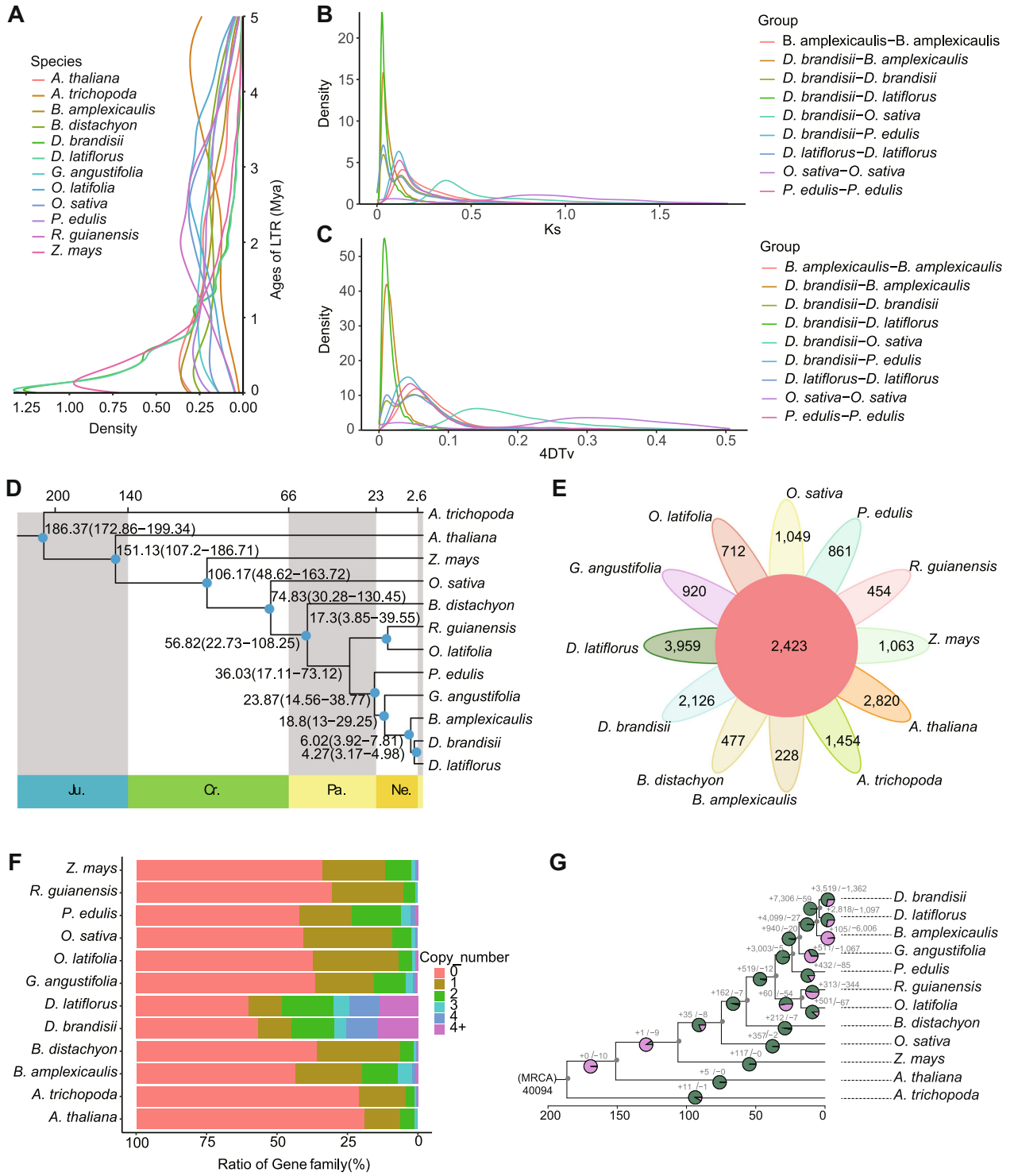

Figure 2. Evolutionary analysis of the *Dendrocalamus brandisii* genome

(A) Density plot showing the burst of long terminal repeats (LTRs) in the indicated species. **(B)** Density plot showing pairwise synonymous substitutions (Ks) values between the indicated pairs of genomes. **(C)** Density plot showing pairwise four-fold synonymous (degenerative) third-codon transversion (4DTv) values between the indicated pairs of genomes. **(D)** Phylogenetic tree of 12 plant species, with the predicted divergence time shown as each branch. **(E)** Petal plot showing the overlapping (center circle) and specific (individual petals) gene families among the 12 species. **(F)** Proportion of gene families as a function of copy number among 12 species. **(G)** Evolutionary history of gene family expansion (shown in purple) and contraction (shown in green) among 12 species. The size and color of the circles represent the proportion of genes.

on the divergence times (Figure 2D), we estimate that paleotropical woody bamboos first underwent one WGD event (9–9.79 MYA) simultaneously, followed by the successive divergence of *B. amplexicaulis* (6.02 MYA), *D. brandisii*, and *D. latiflorus* (4.27 MYA). Subsequently, there was one more WGD event (2.4–2.5 MYA) at the same time for *D. brandisii* and *D. latiflorus*, but not for *B. amplexicaulis*. The most recent WGD event did not occur in *B. amplexicaulis*.

To further investigate the genomic evolutionary patterns of *D. brandisii*, we selected 1,633 single-copy genes from the three bamboo species *B. amplexicaulis*, *D. brandisii*, and *D. latiflorus* and from another nine plant species, with which we reconstructed a phylogenetic tree (Figure 2D). The tree indicated that *D. brandisii*, a paleotropical woody bamboo species, is most closely related to *D. latiflorus* and *B. amplexicaulis* (Figure 2D). Indeed, we observed a global collinearity among *D. brandisii*, *B. amplexicaulis*, and *D. latiflorus* (Figure S2). Additionally, we also observed global collinearity of *D. brandisii* with the *P. edulis* and rice genomes (Figure S2).

We compiled a list of all gene families in the above 12 plant species: a pairwise comparison of their numbers, as illustrated by a petal plot, indicated 2,423 gene families being shared among all species, with another 2,126 gene families being present specifically in the *D. brandisii* genome (Figures 2E, S3A). We subjected the gene families specific to *D. brandisii* to a GO term enrichment analysis, which unveiled enrichment in the biological processes "negative regulation of translation", "transposition", "DNA biosynthetic process", "photosynthetic electron transport in photosystem", "positive regulation of translational termination", "positive regulation of translational elongation", "tryptophanyl-tRNA aminoacylation", and "sesquiterpenoid biosynthetic process" (Figure S3B). In terms of molecular function, we observed an enrichment of the gene families specific to *D. brandisii* for "RNA/DNA-directed DNA polymerase activity" (Figure S3C). For GO terms related to cellular component, "he proteasome core complex" and "translation preinitiation complex" were enriched (Figure S3D). KEGG pathway enrichment analysis revealed an enrichment for "protein export", "photosynthesis", and "glucosinolate biosynthesis" (Figure S3E).

Taking a closer look at gene families, we counted the number of gene copies per gene family for every species. We classified all gene families according to their copy number in each species, from zero to four copies, and those exceeding four copies. *D. brandisii* and *D. latiflorus* had the highest proportion of gene families with two or more gene copies (Figure 2F). Expanded gene families were predominant in *D. brandisii* and *D. latiflorus*, whereas we largely only identified contracted gene families in *B. amplexicaulis* (Figure 2G). Specifically, *D. brandisii* had 3,519 expanded gene families and 1,362 contracted gene families, similar to *D. latiflorus* (expansion, 2,818; contraction, 1,097). The contracted gene families were primarily associated with the GO biological process terms "ion transmembrane transport", "water transport", "polyamine biosynthesis", "mRNA polyadenylation", "Rab protein signal transduction", "protein secretion", "protein sumoylation", and "regulation of exocytosis" (Figure S4). By contrast, the expanded gene families were mainly involved in the GO biological process terms "recognition of pollen", "cell surface receptor signaling pathway", "telomere maintenance", "glutathione metabolic process", "mitochondrial gene expression", "intercellular transport", and "cell wall macromolecule catabolic process" (Figure S5).

Overview of the transcriptome atlas of *D. brandisii*

We chose 15 tissue types from *D. brandisii* plants, each represented by three biological replicates, for sequencing of full-length transcripts by Oxford Nanopore long-read technology and produce an extensive transcriptome dataset (Figure 1). These tissues encompassed six different aboveground organs: sheath (T-SHE), culm (T-S), leaf (T-L), flower (T-F), buds at the base of the culm (T-BB), and branch (T-B); as well as three root organs: root primordium (TBRC), root tip (TBR), and root base (T-R). Additionally, we included three bud developmental stages: bud primordium (TBLB), current-year bud (TBLBC), and annual bud (TBLBY). Lastly, we analyzed three distinct parts of 50-cm tall shoots: the base (T-SH-B, at the soil level), middle (T-SH-M), and upper (T-SH-U, including the apical meristem). The number of long reads ranged from 2,097,152 to 6,032,837 across tissues. We polished the full-length sequences within each dataset by using Illumina RNA-seq reads to correct errors and mapped these transcripts back to the genome assembled above for downstream analysis. Principal component analysis and correlation analysis of the samples demonstrated excellent reproducibility within groups and clear differentiation between groups (Figure 3A, B). Notably, the three bud developmental stages (TBLB, TBLBC, and TBLBY) clustered together, as did the three parts of shoots (T-SH-B, T-SH-M, and T-SH-U). This clustering pattern is particularly intriguing in sympodial bamboos such as *D. brandisii*, where buds at the base of the stem are precursors for shoot development. These buds can develop into bamboo shoots, while young branches may have the potential to develop into root structures. Our transcriptome data provide valuable insights to support this hypothesis.

Gene expression and post-transcriptional regulation in the *D. brandisii* shoot by Oxford Nanopore long-read sequencing

D. brandisii shoots are of exceptional quality; thus, we focused on them here (Figure 3C). We produced paraffin sections of shoots at different positions along the top 50 cm, which revealed substantial cell elongation in the base (T-SH-B) and middle (T-SH-M) regions of the shoot. Conversely, the upper (T-SH-U) region of the shoot tip exhibited a compact arrangement of cells with a visible condensed nucleus, indicative of active cell division. The mapping rates of the full-length transcripts obtained for the base (T-SH-B), middle (T-SH-M), and upper (T-SH-U) regions of the shoot were 90.1%, 91.1%, and 92.1%, respectively, suggesting that the *D. brandisii*

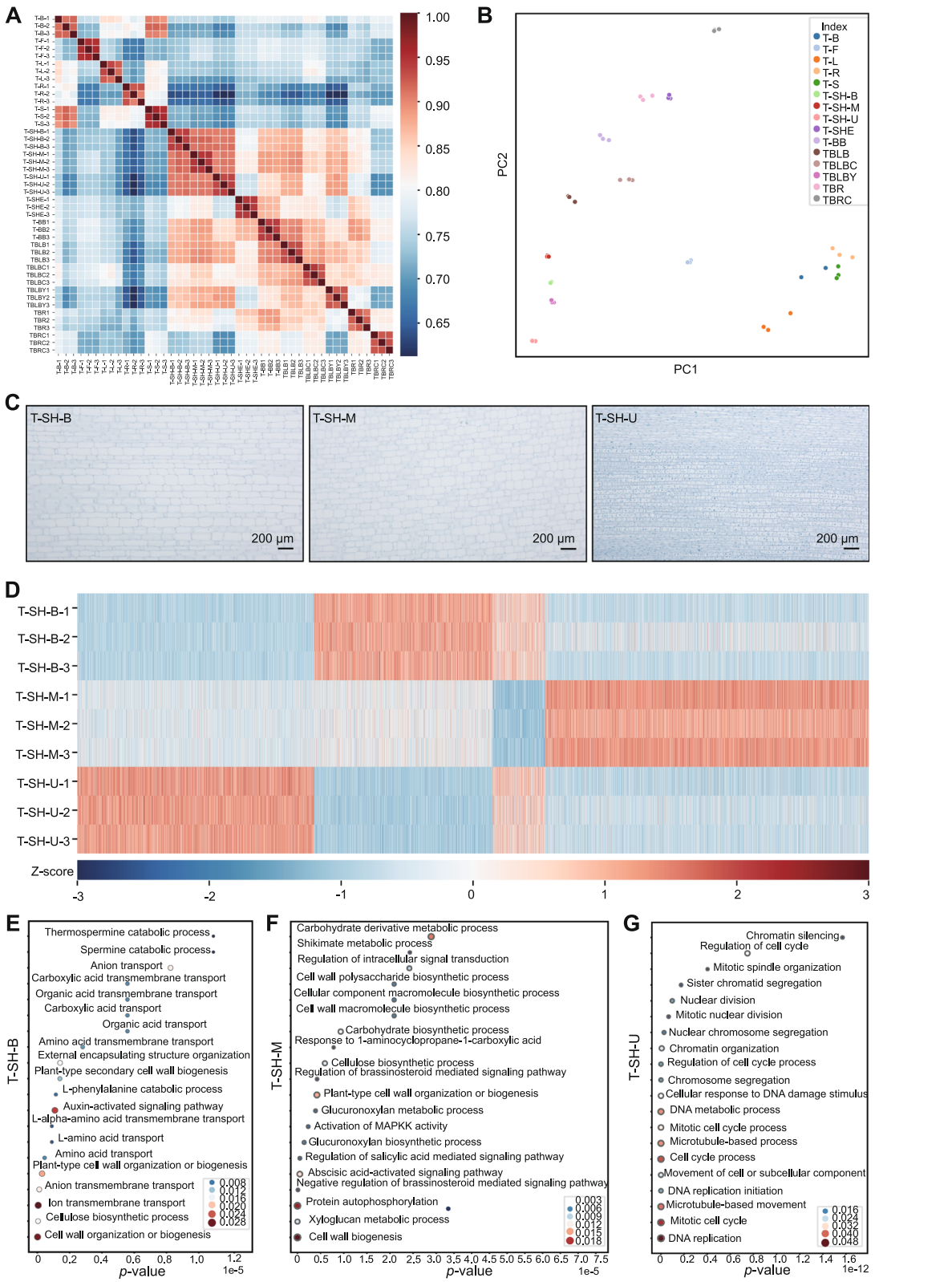

Figure 3. Overview of the transcriptome atlas of *Dendrocalamus brandisii* and paraffin sections of shoots

(A) Heatmap showing the Pearson's correlation coefficients between all pairwise comparisons of replicates and tissue type. **(B)** Principal component analysis of all replicates and tissue samples. **(C)** Representative images of paraffin sections from the base, middle, and upper regions of *D. brandisii* shoots. Scale bars, 200 μm. **(D)** Heatmap representation of the relative expression levels of genes with high expression in the base, middle, and/or upper regions of *D. brandisii* shoots. **(E–G)** List of enriched Gene Ontology (GO) terms for highly expressed genes in the base region **(E)**, middle region **(F)**, or upper region **(G)** of *D. brandisii* shoots.

genome assembly represents most of the transcribed regions captured by Nanopore long-read sequencing. We identified 2, 731 differentially expressed genes (DEGs) (502 upregulated, 2,229 downregulated) between the middle and the base of the shoot, and 4,231 DEGs (2,983 upregulated, 1,248 downregulated) between the upper and middle regions of the shoot. A heatmap and clustering analysis of all DEGs revealed three distinct gene clusters with higher expression levels specifically in T-SH-B, T-SH-M, or T-SH-U (Figure 3D). We subjected the upregulated DEGs that are specific to each part of the shoot to a GO term enrichment analysis: the upregulated DEGs specific to the basal part of the shoot were primarily enriched in processes related to "plant-type cell wall biogenesis" and "callose deposition in cell wall" (Figure 3E). The DEGs specifically upregulated in the middle part of the shoot were enriched in terms related to various signaling pathways (Figure 3F), while the upregulated DEGs in the upper part of the shoot were associated with cell division (Figure 3G). This analysis indicates that different parts of the *D. brandisii* shoot exhibit differentiated functions during development, with cell cycle and nuclear division being more concentrated in the upper portion of the shoot.

Post-transcriptional regulation mainly includes alternative polyadenylation (APA) and alternative splicing (AS). APA of precursor messenger RNAs (mRNAs) plays a major role in transcriptome diversity (Abdel-Ghany et al., 2016). Among the three shoot samples (T-SH-B, T-SH-M, and T-SH-U), 10,170 genes had a single polyadenylation site (Figure 4A); these genes showed an enrichment for GO terms related to photosynthesis (Figure S6A). Another 22,073 genes exhibited APA events with two or more polyadenylation sites; these genes showed an enrichment for GO terms related to mRNA binding and splicing (Figure S6B). An inspection of the 200 bp of sequence centered on each poly(A) cleavage site revealed an AU-rich composition close to the cleavage site, indicating their authenticity (Figure 4B). In total, we identified 10,185 differential APA events through pairwise comparisons of the T-SH-B, T-SH-M, and T-SH-U samples (Figure 4C). For example, the gene DhA07G023870 associated with an integral membrane component had three putative polyadenylation sites, of which distal polyadenylation sites were prominent in the T-SH-U samples (Figure 4D).

Alternative splicing is a crucial mechanism that contributes to increased complexity and diversity of protein isoforms in plants (Filichkin et al., 2010). Similar to other plant species, AS in *D. brandisii* mostly consisted of intron retention (IR) (Figure 4E–G). The order from highest to lowest occurrence was IR > alternative 5′ splice site (A5SS) > alternative 3′ splice site (A3SS) > exon skipping (ES) > mutually exclusive exon (MEE). We identified differential AS events in pairwise comparisons between the T-SH-B, T-SH-M, and T-SH-U samples (Figure 4H). For example, DhA03G020950, encoding an RNA-binding protein with an NFACT-R domain, exhibited partial retention of its third intron in all shoot samples, but with the T-SH-B and T-SH-M samples showing a lower overall splicing efficiency of this intron compared to the T-SH-U sample (Figure 4I). Investigating whether differential post-transcriptional regulation regulates bamboo shoot development will be an important future research goal.

Analysis of the small RNAome of *D. brandisii* shoots

To explore the transcriptional regulatory patterns in different sections of bamboo shoots, we conducted separate small RNA sequencing analysis on the base, middle, and upper segments of 50-cm tall bamboo shoots. We produced 280.73 million clean reads, with each of the three tissue samples having at least 27.79 million clean reads. The size distribution of all small RNA species ranged from 18 to 26 nt. After removing duplicates, we discovered that 24-nt small RNAs are the most frequent in each sample (Figure 5A). Furthermore, the abundance of microRNAs (miRNAs) increased with increasing proximity to the shoot tip (Figure 5B). Additionally, we identified significantly differentially abundant miRNAs in the pairwise comparisons T-SH-M versus T-SH-B, T-SH-U versus T-SH-B, and T-SH-U versus T-SH-M (Figure 5C, D). The greatest number of differentially abundant miRNAs occurred between the T-SH-M and T-SH-B samples (Figure 5D). Clustering analysis of all differentially abundant miRNAs revealed that the abundance of miRNAs in one of the clusters gradually increased from the base to the tip of the shoot, such as with miR390 (Figure 5E), which might be associated with auxin-related genes in the shoot. Conversely, the abundance of miRNAs in other clusters gradually decreased from the base to the tip of the shoot, such as with miR168 and miR396 (Figure 5F). We also observed high abundance for miR166 in the T-SH-M samples; miR166 potentially targets the transcript of DhA05 G023140, encoding a serine/threonine kinase. In agreement, DhA05 G023140 transcript levels were low in the T-SH-M samples.

We next aimed to identify the target transcripts for all differentially abundant miRNAs. Specifically, we looked for more abundant transcripts and less abundant miRNAs across the T-SH-B, T-SH-M, and T-SH-U samples. In the base of bamboo shoots, the main functions of the resulting miRNA–gene network were related to "phenylalanine biosynthesis," "plant–pathogen interactions," and "flavonoid biosynthesis" (Figure 5G). In the middle part of the shoot, we identified a distinct set of connections between miRNAs and genes, which were involved in processes such as "material transport", "energy metabolism", and "signal transduction" (Figure 5G). In the upper part of the shoot, the miRNA–gene network was largely related to "DNA replication" and "cell division" (Figure 5G). Numerous DEGs encoding growth regulation factors were among the targets of miRNAs in the middle and upper parts of bamboo shoots, suggesting a higher concentration of growth and developmental regulators in these regions.

Lignin biosynthetic characteristics and metabolite differences between *D. brandisii* and *P. edulis* shoots

The concentration and composition of lignin in bamboo play pivotal roles in determining the taste and dietary fiber content

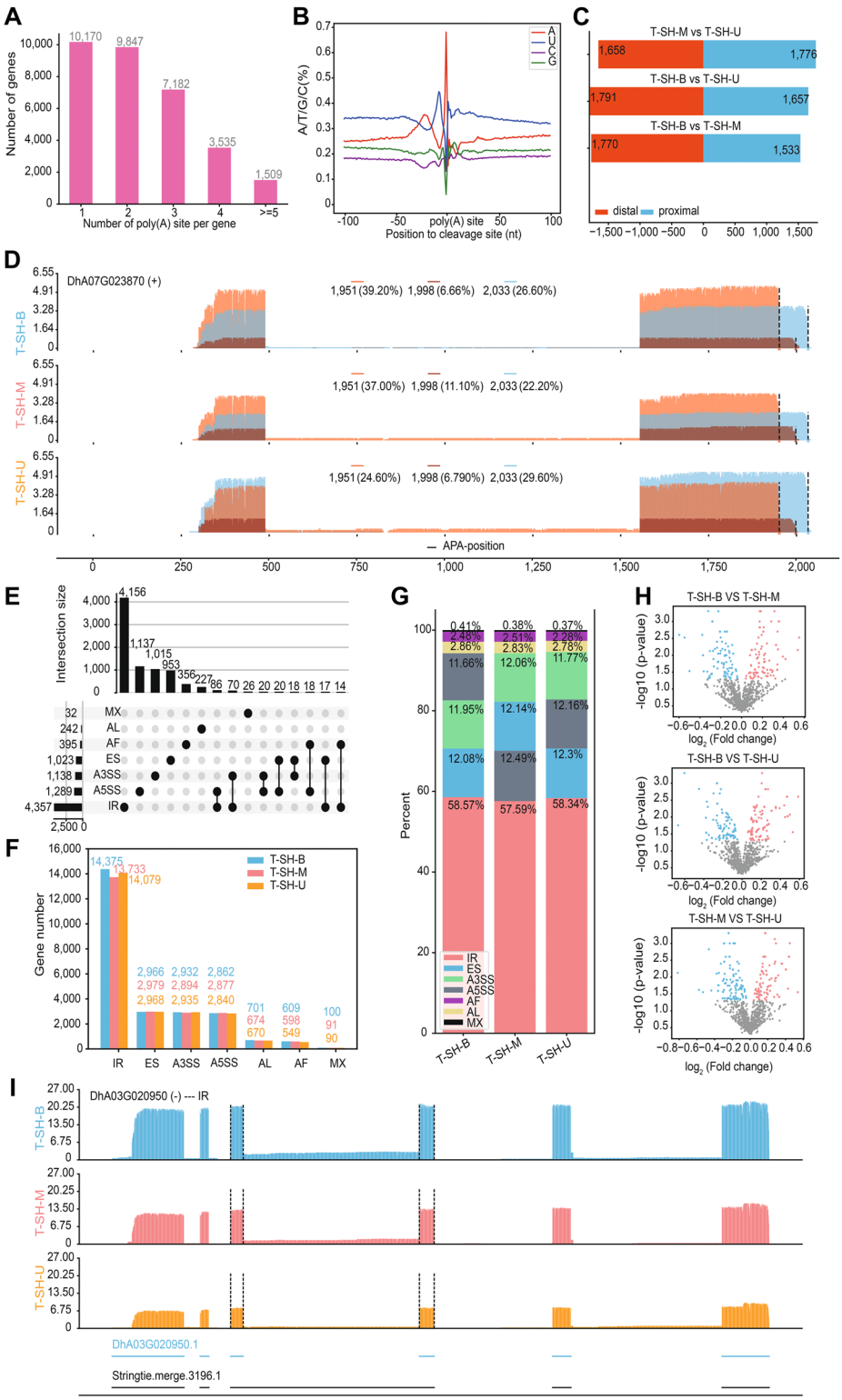

Figure 4. Overview of post-transcriptional regulation of the *Dendrocalamus brandisii* shoot transcriptome

(A) Histogram showing the number of genes with multiple poly(A) sites. **(B)** Sequence preference around poly(A) cleavage sites. **(C)** Histogram showing the number of differential alternative polyadenylation (APA) events through pairwise comparisons of T-SH-B (base of the shoot), T-SH-M (middle part of the shoot), and T-SH-U (upper part of the shoot). **(D)** Wiggle plots showing the relative abundance of transcripts with one of the three detected poly(A) sites of DhA07G023870 in the T-SH-U, T-SH-M, and T-SH-B samples. **(E)** Upset plot showing the number of alternative splicing (AS) events. **(F)** Histogram showing the number of genes with different types of AS events. **(G)** Percentage of different AS types in the T-SH-B, T-SH-M, and T-SH-U samples. **(H)** Volcano plots showing differential AS events in the indicated pairwise comparisons. Blue dots indicate less abundant differential AS events; red dots indicate more abundant differential AS events. **(I)** Wiggle plots showing differential splicing of DhA03G020950 intron three.

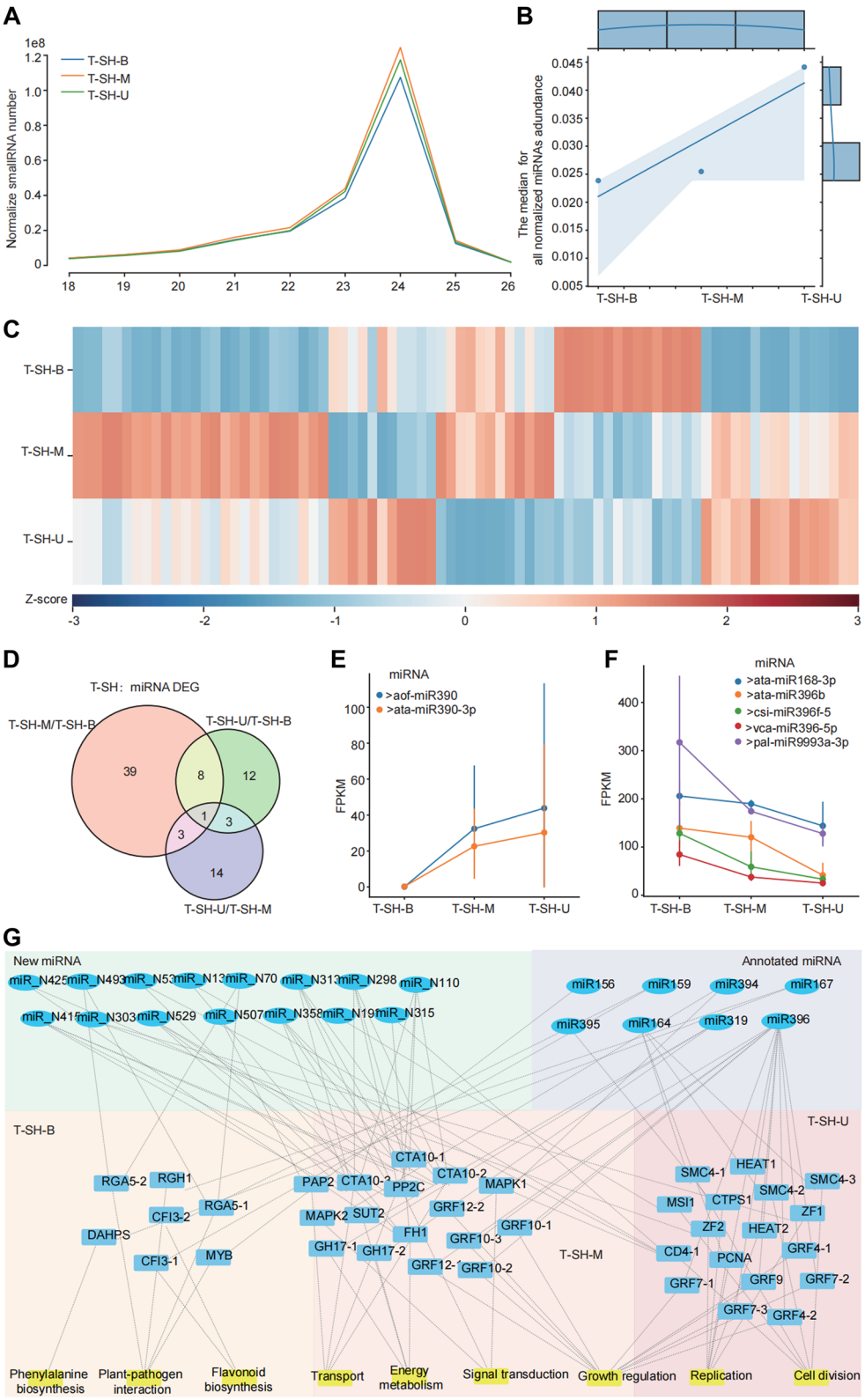

Figure 5. Analysis of the small RNAome of *Dendrocalamus brandisii* shoots

(A) Normalized number of small RNAs as a function of length (in nucleotides) in the T-SH-B, T-SH-M, and T-SH-U samples. **(B)** Relative normalized abundance of microRNAs (miRNAs) in the three shoot tissue types. **(C)** Heatmap representation of relative miRNA abundance in the three shoot tissue types. **(D)** Venn plot showing the extent of overlap among differentially abundant miRNAs in each of the three shoot tissue types. **(E, F)** Abundance of miR390 **(E)** and miR168, miR396, and miRNA9993a **(F)** in the three shoot tissue types. **(G)** Network showing newly identified and previously annotated miRNAs, their target genes, and their target gene networks.

of its shoots, as well as the quality and applicability of bamboo as timber. Genes encoding the key lignin biosynthetic enzymes 4-coumarate:coenzyme A ligase (4CL), cinnamoyl-CoA reductase (CCR), and ferulate 5-hydroxylase (F5H) were expressed at higher levels in *P. edulis* than in *D. brandisii* (Figure 6A). F5H serves as the principal rate-determining enzyme, governing the conversion of guaiacyl lignin precursors to syringyl lignin precursors. We used the

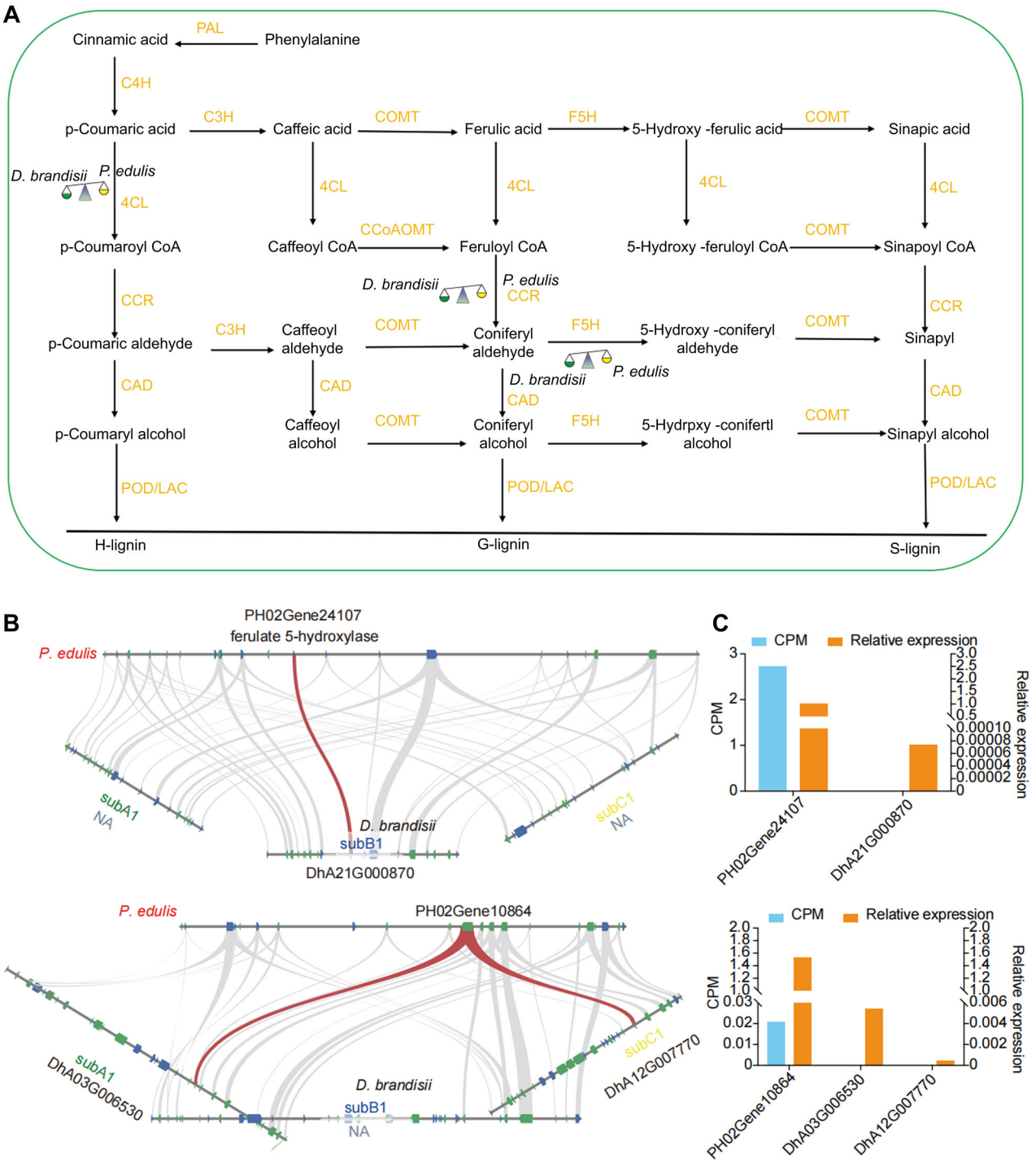

Figure 6. Synteny and expression of *Ferulate 5-hydroxylase* in *Dendrocalamus brandisii* shoots

(A) Lignin biosynthesis pathway. The green and yellow droplets on either side of the scale respectively represent their expression levels in *D. brandisii* and *Phyllostachys edulis*. **(B)** Collinearity analysis of *ferulate 5-hydroxylase* (PH02Gene24107 and PH02Gene10864) from *P. edulis* and the three subgenomes of *D. brandisii*. **(C)** Relative expression levels of PH02Gene24107 and PH02Gene10864 from transcriptome data and those of the collinear genes on each of the subgenomes of *D. brandisii*, as determined by reverse transcription – quantitative polymerase chain reaction (RT-qPCR). CPM, counts per million.

P. edulis sequence for *F5H* to perform a microsynteny gene pair analysis against the *D. brandisii* genome, which identified two collinear gene pairs of F5H between the two bamboo species (Figure 6B). We obtained RNA-seq data for shoot samples collected from *P. edulis* (Li et al., 2018) and compared the expression levels of all genes participating in the lignin biosynthesis pathway between *P. edulis* and *D. brandisii. F5H* was generally expressed at a low level in *D. brandisii*. *F5H* expression was higher in the *P. edulis* samples than in *D. brandisii*, as determined by reverse transcription quantitative polymerase chain reaction (RT-qPCR) analysis (Figure 6C). Thus, the slightly higher expression of *F5H* in *P. edulis* shoots relative to those of *D. brandisii* suggests that *P. edulis* may produce more G-type lignin, while *D. brandisii* shoots may accumulate lower levels of G-type lignin. This difference in lignin composition may be one of the reasons why *D. brandisii* shoots are more palatable and have a longer period of edibility than those of *P. edulis*.

The edibility of bamboo shoots is a crucial economic trait, and *D. brandisii* shoots are widely recognized as the most delicious and edible among various bamboo species. Therefore, we performed a comparative metabolomic analysis of *D. brandisii* shoots and shoots from *P. edulis*, which are another important edible bamboo species (Figure 7A). This metabolomic analysis identified 990 metabolites in *D. brandisii* shoots and 909 metabolites in *P. edulis* shoots, with 561 shared metabolites between the two species (Figure 7B). We conducted a differential metabolite analysis and identified 475 differential metabolites between the two species, with 269 more abundant metabolites and 206 less abundant metabolites in *D. brandisii* shoots relative to *P. edulis* shoots (Figure 7C). The top 10 most differentially abundant metabolites were mainly 4′-hydroxy-5,7-dimethoxyflavanone, 5,7,4′-trihydroxy-3′,5′-dimethoxyflavone, 4′,5,7-trihydroxy-3′,6-dimethoxyflavone, L-tryptophan, vanillic acid, and L-Valyl-L-Phenylalanine (Figure 7D). Flavonoids and alkaloids were the primary metabolites showing variations between *D. brandisii* and *P. edulis*, with *D. brandisii* exhibiting a higher proportion of flavonoids (12.7% compared to 9.8% for *P. edulis*) but a lower content of alkaloids (7.6% compared to 9.7% for *P. edulis*). Additionally, *P. edulis* had higher levels of bitter amino acids such as phenylalanine (Phe), valine (Val), leucine (Leu), and isoleucine (Ile). This finding suggests that the taste difference between *D. brandisii* and *P. edulis* can be attributed to disparities in their amino acid, alkaloid, and flavonoid contents.

Moreover, we detected differences in the contents of D-glucose and D-fructose, with *D. brandisii* having higher levels of both sugars in its shoots than *P. edulis* (Figure 7E, F). Using genes related to fructose metabolism from *P. edulis* as a starting point, we performed a microsynteny analysis, which revealed several collinear gene pairs associated with fructose metabolism between the two bamboo species (Figure 7G). Among them, genes encoding the enzymes glutamine--fructose-6-phosphate aminotransferase, fructose-bisphosphate aldolase 1, and fructose 6-phosphate 1-phosphotransferase subunit alpha were more highly expressed in *D. brandisii* than in *P. edulis* (Figure 7H). In conclusion, the excellent taste of *D. brandisii* shoots can be attributed primarily to their high flavonoid contents and low alkaloid contents. Additionally, the elevated sugar contents and the presence of palatability-related substances also partly contribute to their desirable edible characteristics.

DISCUSSION

Bamboo, the largest type of grass in the world, comprises a single evolutionary radiation of 1,642 species, including 1,521 woody bamboo. Bamboo, a common plant with exceptional properties, has been intricately linked with human civilization since antiquity. In contemporary society, the role of bamboo as a construction material is often highlighted, while its significance as a food source is frequently underappreciated, despite its enduring role over centuries as a critical food and medicinal resource for both animals and humans. Importantly, for certain species like the giant panda and the golden bamboo lemur, bamboo represents the only source of food. However, only six bamboo genomes have been sequenced thus far; of these, only two have been assembled at the chromosome level, resulting in limited knowledge about bamboo shoot formation and growth mechanisms and hindering the development of bamboo utilization and industry (Peng et al., 2013; Zhao et al., 2018; Guo et al., 2019; Zheng et al., 2022). An in-depth molecular characterization of *D. brandisii*, known for its high-quality shoots, is crucial for exploring the growth regulation and improving bamboo shoot quality. Thus, genome sequencing of *D. brandisii* needed to be addressed. In this study, we obtained a high-quality genome assembly for *D. brandisii* (2,756,032,269 bp with contig N50 values of 15.19 Mb), consisting of three subgenomes, slightly larger than the genome of *D. latiflorus*. Comparative genomics analysis revealed that the genomes of hexaploid bamboos have undergone a recent WGD event. The examination of gene families showing expansion and contraction indicated that *D. brandisii* and *D. latiflorus* have much larger gene families compared to other bamboo species, potentially aiding in their adaptation to the environment after recent genome-wide duplication (Ajayi and Showalter, 2020; Gomez-Perez and Kemen, 2021). However, they differ in gene families related to flower development, suggesting different pathways to flower formation.

To establish the relationship between gene expression patterns and related tissues, we constructed a high-quality transcriptome dataset of 15 tissues to facilitate future studies on *D. brandisii*. Clustering analysis demonstrated a closer relationship between lateral branches and shoots than to other tissues, aligning with the specifics of bamboo biology. *D. brandisii*, being a sympodial bamboo, exhibits high regeneration ability, where lateral branches can be regenerated and develop into new plants through the culm-burying method. This observation suggests that bamboo shoots and lateral branches might have overlapping functions, but

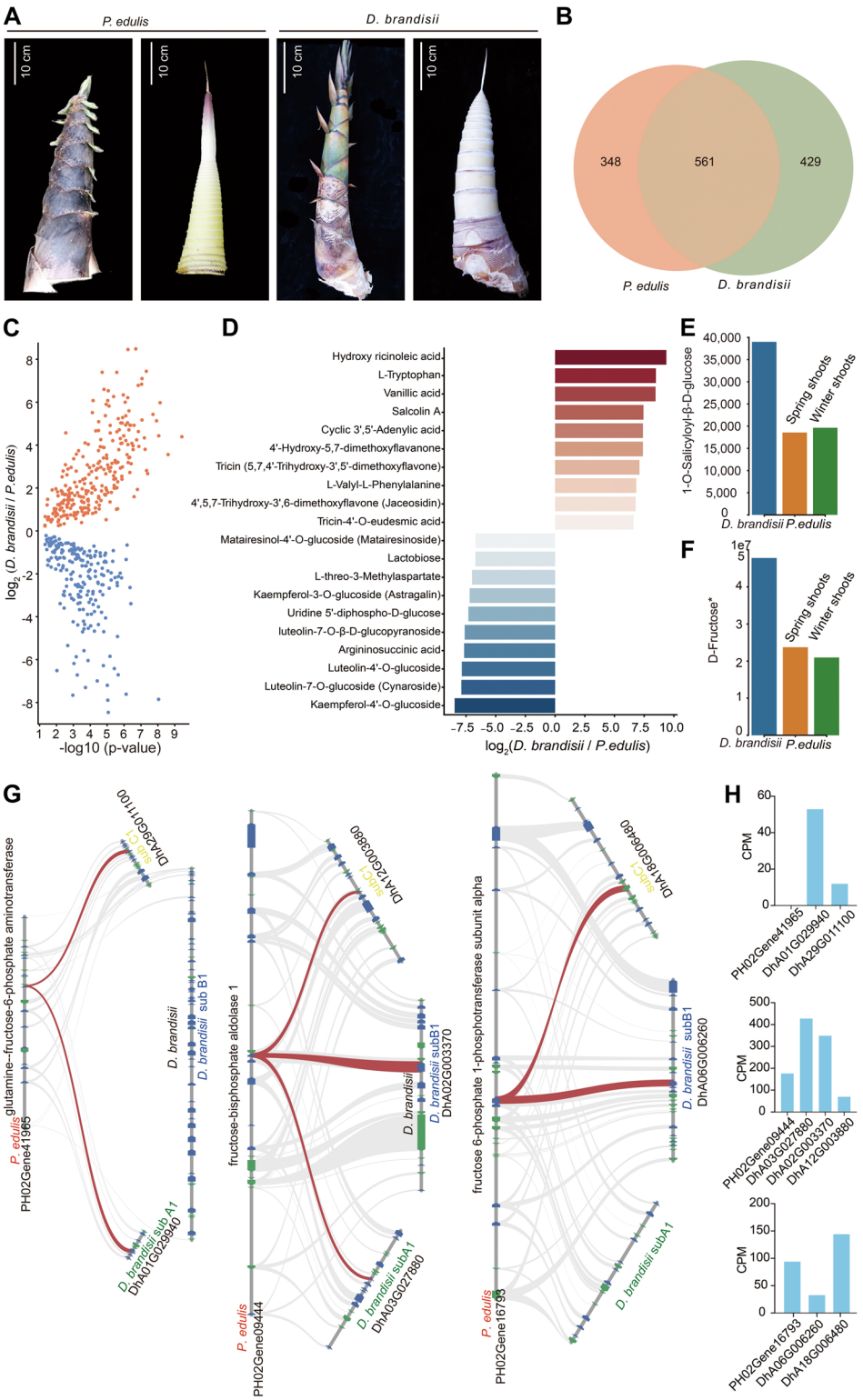

Figure 7. Metabolite profiling of *Dendrocalamus brandisii* and *Phyllostachys edulis* shoots

(A) Representative photographs of shoots from *D. brandisii* and *P. edulis* used for metabolome profiling. Scale bars, 10 cm. **(B)** Venn diagram showing the overlap between metabolites detected in both species. **(C)** Volcano plot showing the differentially abundant metabolites between *D. brandisii* and *P. edulis* shoots. Red circles indicate more abundant metabolites in *D. brandisii*; blue circles indicate less abundant metabolites in *P. edulis*. **(D)** Histogram showing the top 10 differentially abundant metabolites. **(E, F)** Content of 1-O-salicyloyl-β-D-glucose **(E)** and D-fructose **(F)** in *D. brandisii* shoots and two different stages of *P. edulis* shoots (winter shoots and spring shoots). **(G)** Collinearity relationships among the genes encoding fructose 6-phosphate 1-phosphotransferase subunit beta, 6-phosphofructokinase 1, and fructose-bisphosphate aldolase 3 from *P. edulis* and the three subgenomes of *D. brandisii*. **(H)** Relative expression levels of the genes shown in **(G)**, as determined by RNA-seq analysis. CPM, counts per million.

the regulatory mode and expression of related genes during specific bamboo developmental stages will require further exploration. Moreover, we examined genes with high expression levels in different segments of the shoot and discovered notable variations in function. The upper part of the shoot appears to be more involved in cell division, while the base and middle portion of the shoot tend to be associated with cell wall biogenesis. These findings provide guidance for future shoot function-related studies.

In contrast to many other agricultural crops, bamboos flourish naturally with minimal human intervention, demonstrating an impressive resilience to diseases, pests, and weather-related challenges, and thrive without the need for fertilizers or pesticides. Furthermore, bamboo shoots remain free from residual toxicity, as they are protected by multiple layers of tightly clasped sheaths, thus sheltering from surrounding pollutants. The extraction and identification of numerous nutritious and bioactive constituents, such as vitamins, amino acids, proteins, phenolic acids, polysaccharides, trace elements, and steroids, from bamboo shoots revealed their health benefits, including antioxidant, anti-aging, anti-bacterial, and anti-viral properties (Nirmala et al., 2007; Chongtham et al., 2011a; Pandey and Ojha, 2013). As a result of these favorable chemical properties and the capacity of bamboo to address various global challenges, bamboo shoots are currently experiencing unprecedented interest worldwide. Over the past decade, despite a global economic downturn, the international trade in bamboo shoots has continued to grow steadily, with an export growth rate of 3.85%. Asia has emerged as the continent with the largest volume of bamboo shoot exports, totaling US $1.71 million and accounting for approximately 62.5% of the global trade volume (Figure S7) (Comtrade, 2022).

D. brandisii is recognized for its excellent shoot quality. While *D. brandisii*, one of the major sweet bamboo species, produces shoots in the summer, Moso bamboo produces shoots in the spring; this seasonal difference may contribute to variations of various aspects of their shoots. Moreover, Moso bamboo and *D. brandisii* have different natural distribution areas; therefore, it cannot be ruled out that these differences exist due to factors such as climate and soil. The distribution range of Moso bamboo is extensive, ranging from the western Guangxi to the eastern Fujian and Zhejiang, and further inland to Anhui. However, it exhibits no taste differences. Based on practical production experience from transplantation experiments, it has been observed that *D. brandisii* consistently maintains excellent shoot quality wherever it manages to survive, indicating that it is not influenced by environmental factors. To investigate the differences in shoot quality between bamboo species, we conducted a comparative metabolomic analysis between *D. brandisii* shoots and *P. edulis* shoots (winter shoots and spring shoots as separate samples), which are also edible. The results revealed variations in the composition of various metabolites, particularly alkaloids and flavonoids, between the two bamboo species. Differential metabolites analysis revealed that flavonoids are less abundant in *D. brandisii* shoots compared to *P. edulis* shoots. Additionally, we analyzed the expression of *F5H*, related to lignin biosynthesis; *F5H* was less expressed in *D. brandisii* shoots than in *P. edulis* shoots, which may contribute to a lower content of S-type lignin in *D. brandisii* shoots, which may be related with their superior quality (Hendra et al., 2011; Martins et al., 2015; Huang et al., 2022). The gene regulatory networks underlying bamboo shoot edibility will remain a main focus of research.

Bamboo shoots are more than just a natural delicacy; they are a nutrient-rich and wholesome food choice that aligns seamlessly with contemporary dietary trends. Among the various bamboo species, *Dendrocalamus* species are distributed worldwide (Table S1, https://doi.org/10.15468/DL.879ZRT) (User, 2023), although *D. brandisii* is now less commonly distributed (Table S2, https://doi.org/10.15468/dl.tp4br7) (User, 2023); it belongs to the genus *Dendrocalamus*, suggesting that it may adapt well to climatic environments similar to those populated by other *Dendrocalamus* species. In China, this species has gained widespread popularity owing to its exceptional taste and outstanding quality. Originally cultivated in the Yunnan Province, its cultivation has now extended to the provinces of Guangdong, Sichuan, Guangxi Zhuang Autonomous Area, and Chongqing City. Additionally, simple greenhouse cultivation has been initiated in regions such as Zhejiang, Jiangsu, and Beijing city. To further enhance *D. brandisii* cultivation, it is anticipated that this particular bamboo species will continue to gain a larger market share in the bamboo shoot industry in the future.

In this work, we assembled a high-quality genome assembly for the heterozygous hexaploid species *D. brandisii*, and used Oxford Nanopore long-read sequencing to construct a comprehensive transcriptome dataset encompassing 15 tissues for gene annotation, revealing differential gene expression and post-transcriptional regulation. By integrating metabolomic data, we revealed how differences in lignin formation, along with abundant flavonoids and fructose, help distinguish *D. brandisii* edible shoots from those of the other edible bamboo species *P. edulis*. Using a multi-omics integrative approach, we uncovered the regulatory mechanisms underlying the superior quality of *D. brandisii* shoots at the genetic, transcriptional, and metabolic levels. The taste quality of bamboo shoots is regulated by a synergistic interplay of multiple factors, rather than being controlled by a single determinant. The high-quality chromosome-level genome, comprehensive transcriptome data, and expansive metabolomic data generated in this study provide insights into the taste quality of bamboo shoots and provide a wealth of reliable omics data for future comprehensive research on bamboo shoots.

MATERIALS AND METHODS

Plant material collection

All of the bamboo materials used in this study were collected from Pu'er City, Yunnan Province (100.94370° E, 22.72578° N), which is the natural distribution area of *D. brandisii*.

The bamboo materials collected include: young leaves (for genome sequencing), mature leaves, roots, culms, flowers, lateral buds, current-year lateral buds, annual lateral buds, lateral branches, sheaths, bamboo buds at the base of culm, the base, middle, and upper portions of 50-cm tall bamboo shoots, the root base, and root tips. For each biological replicate, six plant samples were combined, for a total of three replicates. To ensure RNA integrity, all samples were immediately subjected to snap-freezing in liquid nitrogen, followed by transport on dry ice, and then storage at −80°C.

Paraffin sections of *D. brandisii* shoots

After fixing the upper, middle, and lower sections of bamboo shoots in formalinacetic acid-alcohol (FAA), several steps were carried out including dehydration through a graded ethanol series, sample clearing, wax infiltration, and embedding. Slices were then obtained using a microtome to a thickness of 8–10 μm (LIECADEM2135, Germany). The slices were placed on microscope slides and then stained with hematoxylin-eosin; the slides were mounted in Canada balsam, and subsequently examined using a microscope (Leica MC170 HD, Germany).

Genomic DNA extraction, library construction, and genome survey

Genomic DNA was isolated from young leaves by employing a Plant Mini Kit (Qiagen, Hilden, Germany). The purity and concentration of the extracted DNA was assessed using a NanoDrop One UV-Vis spectrophotometer (Thermo Fisher Scientific, USA). High-grade genomic DNA was subsequently fragmented to a target size of 350 bp in preparation for constructing a DNA sequencing library. Following rigorous quality control procedures, the library was then submitted for paired-end sequencing with a read length of 150 bp on an Illumina instrument. The resulting sequencing data were subjected to quality controls to generate clean reads. The resulting high-quality clean reads were processed using Jellyfish (v2.1.4) and GenomeScope (v2.0), allowing for the assessment of genome size, assembly of the genome, determination of GC content, and evaluation of heterozygosity (Li et al., 2008, 2010; Vurture et al., 2017).

Genome assembly and chromosome scaffolding

PacBio libraries (15-kb insert size) were constructed using genomic DNA, followed by PacBio circular consensus sequencing (CCS). High-quality data were obtained by eliminating low-quality information. The clean CCS data were then assembled using the hifiasm software (Cheng et al., 2021) to yield scaffold sequences. Subsequently, Hi-C libraries were constructed, sequenced, and used to anchor the scaffolds into chromosomes. The library titer was determined using a Qubit 2.0 instrument, while insert size was assessed on an Agilent 2100 instrument. Upon validation, the libraries were sequenced on an Illumina NovaSeq. 6000 instrument to yield paired-end 150-bp reads. The raw data obtained from Hi-C sequencing went through a data filtering step to yield high-quality clean data. HiC-Pro v2.10.0 (Servant et al., 2015) was used to filter and evaluate the Hi-C data. Subsequently, LACHESIS software was used to cluster and order the scaffolds (Burton et al., 2013). Manual mapping and inspection were performed to obtain the final version of the chromosome-level genome assembly. The assembly results were evaluated in three aspects: mapping ratio of Oxford Nanopore long-read RNA-seq, BUSCO evaluation (Parra et al., 2007; Li and Durbin, 2009; Simão et al., 2015) and LAI (Ou et al., 2018) with default parameters.

Annotation of repeat elements and genes

To identify repetitive sequences in the *D. brandisii* genome, RepeatModeler2 (v2.0.1) was used (Flynn et al., 2020) for *de novo* prediction, which mainly employed two repetitive sequences prediction software: RECON (v1.0.8) (Bao and Eddy, 2002) and RepeatScout (v1.0.6) (Price et al., 2005). The predictions were then classified using RepeatClassifier (Flynn et al., 2020), which uses repbase (v19.06) (Jurka et al., 2005), REXdb (v3.0) (Neumann et al., 2019), and Dfam (v3.2) (Wheeler et al., 2012) as reference databases. Additionally, LTR_retriever (v2.8) (Ou and Jiang, 2018) was specifically employed for *de novo* prediction of LTR sequences. The *de novo* prediction results and known databases were merged and collapsed into a NR database of repeat sequences specific to the species. Finally, transposable element (TE) sequences within the genome were predicted using RepeatMasker (v4.1.0) (Chen, 2004) using the established repetitive sequence database above.

For gene prediction, three commonly used approaches were employed. First, *de novo* prediction was carried out using Augustus v2.4 (Stanke et al., 2008) and SNAP (Korf, 2004). Second, a homology search was conducted using GeMoMa v1.7 (Keilwagen et al., 2016) for species-based prediction. Third, transcript-based assembly was performed using Hisat v2.0.4 (Kim et al., 2015), Stringtie v1.2.3 (Pertea et al., 2015), and GeneMarkS-T v5 (Tang et al., 2015). The prediction outcomes derived from the three aforementioned methods were consolidated using Evidence Modeler (EVM) v1.1.1 (Haas et al., 2008).

Phylogenetic analysis

To determine the evolutionary relationship between *D. brandisii* and other plant species, 11 species were selected to reconstruct a phylogenetic tree: *P. edulis*, *D. latiflorus*, *Amborella trichopoda*, *Guadua angustifolia*, *Raddia guianensis*, *Z. mays*, *Oryza sativa*, *Oxalis latifolia*, *Bistorta amplexicaulis*, *Arabidopsis thaliana*, and *Brachypodium distachyon*. A collection of 1,633 single-copy genes was employed to reconstruct a phylogenetic tree, using IQ-TREE v1.6.11 software, with the maximum likelihood (ML) method and 1,000 bootstrap replicates (Nguyen et al., 2015). *A. trichopoda* was selected as the outgroup to establish a rooted phylogenetic tree. The divergence times were computed using the MCMCTREE package included in the PAML v4.9i software (Yang, 1997). The results were visualized with MCMCTreeR v1.1 software (Puttick, 2019).

CAFE v4.2 software was used to assess the changes in the size of gene families, examining both contractions and expansions (Han et al., 2013). To determine significant contractions and expansions of gene families, a threshold had to be met where both family-wide *P*-values and Viterbi *P*-values were required to be less than 0.05. Additionally, positive selection analysis was conducted using the CodeML module within PAML.

Whole-genome duplication was investigated using the synonymous mutation rate Ks method and the 4DTv method (Zwaenepoel and Van de Peer, 2019). Candidate LTR-RT sequences in the genome were identified using LTR_FINDER v1.07 (Xu and Wang, 2007) and LTRharvest v1.5.9 (Ellinghaus et al., 2008). The Kimura model was used, via EMBOSS v6.6.0 software (Rice et al., 2000), to compute the evolutionary distance.

RNA extraction and Nanopore sequencing

Initially, total RNA was isolated using an RNAprep pure Plant Kit (DP432, TIANGEN, China). Complementary DNA (cDNA) libraries were then assembled using a cDNA-PCR sequencing kit (SQK-LSK110 + EXP-PCB096, ONT, England), in accordance with the standard protocol. The procedure involved reverse transcription into first-strand cDNA, addition of switch oligos, synthesis of complementary strands, and purification using magnetic beads. The cDNA library was processed on a Nanopore sequencing platform. The transcriptome consisting of full-length transcript sequences was obtained by following four main steps. First, ribosomal RNA sequences and low-quality reads were removed from the raw data (sequences shorter than 200 bp, Q-score below 6). Second, full-length sequences were identified by the presence of primers at both ends. Third, the full-length sequences were polished by short reads. Fourth, all sequences were compared and collapsed to a NR consensus based on comparison to *D. brandisii* genome using minimap2 software (Li, 2018). The full-length transcripts identified by Nanopore sequencing were cross-referenced to known transcripts using the gffcompare tool to uncover previously unannotated transcripts and enrich the genome annotation (Geo and Mihaela, 2020).

Alternative splicing analysis based on Nanopore long reads

The Nanopore long reads were mapped onto the reference genome using minimap2 software, applying the command "minimap2 -ax splice" (Li, 2018). The generated Sequence Alignment Map (SAM) files were subsequently managed using samtools, undergoing view, sort, and index operations. The resulting assembled Binary Alignment Map (BAM) files, produced from the minimap2 alignment, were then further processed through Stringtie2 in long-read mode, utilizing the command parameters "-conservative -L." The assembled gene transfer format (GTF) files were compared to the annotation file using the default parameters of gffcompare to establish transcript annotations. The assembled and annotated transcripts were then analyzed for AS events using SUPPA2 (Trincado et al., 2018). The command "suppy generateEvents -e SE SS MX RI FL -f ioe" was used to detect seven different types of AS events. The gffread tool was employed to extract transcript sequences from the *D. brandisii* genome, which were subsequently aligned to the transcriptome via minimap2, using the command "-ax map-ont." The aligned long reads per transcript were enumerated, with expression levels being quantified via reads per million (RPM) normalization. To compute the percent spliced-in (PSI) values for various AS events, the psiPerEvent command from SUPPA2 was used, with default parameters. The diffSplice tool was used for differential analysis of AS events with the following parameters "--method empirical -pa -gc -c." AS events with a *P*-value below 0.05 deemed to represent significant differential AS events.

Alternative polyadenylation analysis

For APA detection, the polyadenylation site (PAS) of each gene was required to have a minimum coverage of five reads and a usage rate of at least 5% to be considered as a candidate PAS. Additionally, a minimum distance of 30 nucleotides (nt) was required between two independent PASs. The PAS with the highest usage rate in each gene was considered the major PAS. Genes in which the major PAS changed between comparison groups were considered to be subjected to APA. The relative positions of the major PASs in the control group were used to determine whether the shift in PAS occurred in the proximal or distal direction. Evaluation of statistical significance used Fisher's exact test, with genes with a *P*-value below 0.05 regarded as having significantly modified PASs (Herrmann et al., 2020). Bedtools software was employed to extract the sequences covering 100 bp upstream and downstream from the PASs, followed by computation of the base content distribution.

Small RNA sequencing and target gene prediction

Nine samples were selected for miRNAs analysis, each comprising three biological replicates from the base, middle, and upper sections of the bamboo shoots. The raw sequencing data, obtained on an Illumina platform, underwent rigorous quality control steps to produce clean data, confirming that the clean data for each individual sample consisted of at least 25 million reads. To identify miRNAs, small RNA reads were compared to the standard miRBase (v22) database using Bowtie software (Langmead et al., 2009). Additionally, new miRNAs were predicted using miRDeep2 software (Friedlander et al., 2012). For target gene identification, both known miRNAs and newly predicted miRNAs were used. For target gene prediction, the miRNA sequences and the transcriptome data generated in this study were combined with TargetFinder software (Allen et al., 2005). Furthermore, differential abundance analysis between sample groups was conducted using edgeR (Robinson et al., 2010) with specific parameters of $|\log_2 (\text{fold-change})| \geq 0.58$ and $P\text{-value} \leq 0.05$.

Metabolomics analysis

The experimental materials used in this study were 50-cm tall shoots of *P. edulis* and *D. brandisii*. Three biological replicates were meticulously prepared. The samples were lyophilized in a freeze-dryer (Scientz-100F), after which they were ground into a fine powder (at 30 Hz for 1.5 min). A 100-mg portion of the powder was suspended in 1.2 mL of 70% (v/v) methanol for extraction. After overnight incubation at 4°C, the mixture was subjected to centrifugation at 12,000 r/min (15,294 *g*) for 10 min to obtain the supernatant. The collected supernatant was then passed through a 0.22-μm filter and collected into an injection vial for ultra-performance liquid chromatography (UPLC) (on a SHIMADZU Nexera X2 platform) and tandem mass spectrometry (MS/MS) analyses. The mass spectrometry data were processed using Analyst v1.6.3 software.

Availability of supporting data

The raw data generated in this study have been deposited in the NCBI Sequence Read Archive under the BioProject accession number PRJNA885281. The assembled genome and the annotation files were uploaded to figshare with DOI:10.6084/m9.figshare.24455197.

ACKNOWLEDGEMENTS

We extend our gratitude to Mr. Xingbo Zhang for supplying the *D. brandisii* materials, and to Dr. Jiaojiao Chen for her diligent collection and organization of the bamboo shoot trade data. This work was supported by the National Key Research and Development Program of China (2021YFD2200505, 2018YFD0600101) and the National Natural Science Foundation of China (32071849).

CONFLICTS OF INTEREST

The authors declare no conflict of interest.

AUTHOR CONTRIBUTIONS

J.G. supervised the project. J.G. and L.G. designed the research and revised the manuscript. Y.B. and J.J. designed the research, performed experiments, analyzed the data, and wrote the manuscript. Z.Z. analyzed the data and wrote the manuscript. X.W. and C.L. provided the Moso bamboo data. Y.D. and R.G. collected references and amended manuscript format. C.W. and H.Z. collected and assembled figures. All authors have read and approved the final version of the manuscript.

Edited by: Huilong Du, Hebei University, China

Received Sep. 13, 2023; **Accepted** Dec. 4, 2023; **Published** Dec. 5, 2023

OO: OnlineOpen

REFERENCES

Abdel-Ghany, S.E., Hamilton, M., Jacobi, J.L., Ngam, P., Devitt, N., Schilkey, F., Ben-Hur, A., and Reddy, A.S. (2016). A survey of the sorghum transcriptome using single-molecule long reads. Nat. Commun. **7:** 1–11.

Ajayi, O.O., and Showalter, A.M. (2020). Systems identification and characterization of β-glucuronosyltransferase genes involved in arabinogalactan-protein biosynthesis in plant genomes. Sci. Rep. **10:** 1–14.

Allen, E., Xie, Z., Gustafson, A.M., and Carrington, J.C. (2005). microRNA-directed phasing during trans-acting siRNA biogenesis in plants. Cell **121:** 207–221.

Bai, Y., Cai, M., Dou, Y., Xie, Y., Zheng, H., and Gao, J. (2023a). Phytohormone crosstalk of cytokinin biosynthesis and signaling family genes in Moso Bamboo (*Phyllostachys edulis*). Int. J. Mol. Sci. **24:** 10863.

Bai, Y., Dou, Y., Xie, Y., Zheng, H., and Gao, J. (2023b). Phylogeny, transcriptional profile, and auxin-induced phosphorylation modification characteristics of conserved PIN proteins in Moso bamboo (*Phyllostachys edulis*). Int. J. Biol. Macromol. **234:** 123671.

Bao, Z., and Eddy, S.R. (2002). Automated *de novo* identification of repeat sequence families in sequenced genomes. Genome Res. **12:** 1269–1276.

Bhandawat, A., Singh, G., Seth, R., Singh, P., and Sharma, R.K. (2016). Genome-wide transcriptional profiling to elucidate key candidates involved in bud burst and rattling growth in a subtropical bamboo (*Dendrocalamus hamiltonii*). Front. Plant Sci. **7:** 2038.

Boeckmann, B., Bairoch, A., Apweiler, R., Blatter, M.C., Estreicher, A., Gasteiger, E., Martin, M.J., Michoud, K., O'Donovan, C., Phan, I., et al. (2003). The SWISS-PROT protein knowledgebase and its supplement TrEMBL in 2003. Nucleic Acids Res. **31:** 365–370.

Burton, J.N., Adey, A., Patwardhan, R.P., Qiu, R., Kitzman, J.O., and Shendure, J. (2013). Chromosome-scale scaffolding of de novo genome assemblies based on chromatin interactions. Nat. Biotechnol. **31:** 1119–1125.

Chen, M., Guo, L., Ramakrishnan, M., Fei, Z., Vinod, K.K., Ding, Y., Jiao, C., Gao, Z., Zha, R., and Wang, C. (2022). Rapid growth of Moso bamboo (*Phyllostachys edulis*): Cellular roadmaps, transcriptome dynamics, and environmental factors. Plant Cell **34:** 3577–3610.

Chen, N. (2004). Using Repeat Masker to identify repetitive elements in genomic sequences. Curr. Protoc. Bioinformatics **5:** 11–14.

Cheng, H., Concepcion, G.T., Feng, X., Zhang, H., and Li, H. (2021). Haplotype-resolved *de novo* assembly using phased assembly graphs with hifiasm. Nat. Methods **18:** 170–175.

Chongtham, N., Bisht, M.S., and Haorongbam, S. (2011a). Nutritional properties of bamboo shoots: Potential and prospects for utilization as a health food. Compre. Rev. Food Sci. Food Saf. **10:** 153–168.

Chongtham, N., Bisht, M.S., and Haorongbam, S. (2011b). Nutritional properties of bamboo shoots: potential and prospects for utilization as a health food. Compre. Rev. Food Sci. **10:** 153–168.

Comtrade, U. (2022). The United Nations Commodity Trade Database. Available from: https://comtrade.un.org/labs/data-explorer/

Dixon, P.G., and Gibson, L.J. (2014). The structure and mechanics of Moso bamboo material. J. R. Soc. Interface **11:** 99.

Ellinghaus, D., Kurtz, S., and Willhoeft, U. (2008). LTRharvest, an efficient and flexible software for de novo detection of LTR retrotransposons. BMC Bioinform. **9:** 1–14.

Filichkin, S.A., Priest, H.D., Givan, S.A., Shen, R., Bryant, D.W., Fox, S. E., Wong, W.-K., and Mockler, T.C. (2010). Genome-wide mapping of alternative splicing in *Arabidopsis thaliana*. Genome Res. **20:** 45–58.

Finn, R.D., Mistry, J., Schuster-Bockler, B., Griffiths-Jones, S., Hollich, V., Lassmann, T., Moxon, S., Marshall, M., Khanna, A., Durbin, R.,

et al. (2006). Pfam: Clans, web tools and services. Nucleic Acids Res. **34:** D247–D251.

Flynn, J.M., Hubley, R., Goubert, C., Rosen, J., Clark, A.G., Feschotte, C., and Smit, A.F. (2020). RepeatModeler2 for automated genomic discovery of transposable element families. Proc. Nat. Acad. Sci. U.S.A. **117:** 9451–9457.

Friedlander, M.R., Mackowiak, S.D., Li, N., Chen, W., and Rajewsky, N. (2012). miRDeep2 accurately identifies known and hundreds of novel microRNA genes in seven animal clades. Nucleic Acids Res. **40:** 37–52.

Gao, Q., Jiang, H., Tang, F., Cao, H.-q., Wu, X.-w., Qi, F.-f., Sun, J., and Yang, J. (2019). Evaluation of the bitter components of bamboo shoots using a metabolomics approach. Food Func. **10:** 90–98.

Geo, P., and Mihaela, P. (2020). GFF utilities: GffRead and GffCompare. F1000Res. **9:** 2020.

Gomez-Perez, D., and Kemen, E. (2021). Predicting lifestyle from positive selection data and genome properties in oomycetes. Pathogens **10:** 807.

Guo, Z., Ma, P., Yang, G., Hu, J., Liu, L., Xia, E., Zhong, M., Zhao, L., Sun, G.L., Xu, Y.X., et al. (2019). Genome sequences provide insights into the reticulate origin and unique traits of woody bamboos. Mol. Plant **12:** 1353–1365.

Haas, B.J., Salzberg, S.L., Zhu, W., Pertea, M., Allen, J.E., Orvis, J., White, O., Buell, C.R., and Wortman, J.R. (2008). Automated eukaryotic gene structure annotation using EVidenceModeler and the program to assemble spliced alignments. Genome Biol. **9:** 1–22.

Han, M.V., Thomas, G.W., Lugo-Martinez, J., and Hahn, M.W. (2013). Estimating gene gain and loss rates in the presence of error in genome assembly and annotation using CAFE 3. Mol. Biol. Evol. **30:** 1987–1997.

He, T.-Y., Zheng, J.-M., Chen, L.-Y., Rong, J.-D., and Zheng, Y.-S. (2020). Complete plastid genome of *Dendrocalamus brandisii* (Poaceae, Bambusoideae). Mitochondr. DNA Part B **5:** 1286–1287.

Hendra, R., Ahmad, S., Sukari, A., Shukor, M.Y., and Oskoueian, E. (2011). Flavonoid analyses and antimicrobial activity of various parts of Phaleria macrocarpa (Scheff.) Boerl fruit. Int. J. Mol. Sci. **12:** 3422–3431.

Herrmann, C.J., Schmidt, R., Kanitz, A., Artimo, P., Gruber, A.J., and Zavolan, M. (2020). PolyASite 2.0: A consolidated atlas of polyadenylation sites from 3′ end sequencing. Nucleic Acids Res. **48:** D174–D179.

Huang, X., Wang, W., Gong, T., Wickell, D., Kuo, L.-Y., Zhang, X., Wen, J., Kim, H., Lu, F., and Zhao, H. (2022). The flying spider-monkey tree fern genome provides insights into fern evolution and arborescence. Nat. Plants **8:** 500–512.

Huerta-Cepas, J., Szklarczyk, D., Heller, D., Hernandez-Plaza, A., Forslund, S.K., Cook, H., Mende, D.R., Letunic, I., Rattei, T., Jensen, L.J., et al. (2019). eggNOG 5.0: A hierarchical, functionally and phylogenetically annotated orthology resource based on 5090 organisms and 2502 viruses. Nucleic Acids Res. **47:** D309–D314.

Jurka, J., Kapitonov, V.V., Pavlicek, A., Klonowski, P., Kohany, O., and Walichiewicz, J. (2005). Repbase update, a database of eukaryotic repetitive elements. Cytogenet. Genome. Res. **110:** 462–467.

Kanehisa, M., Sato, Y., Kawashima, M., Furumichi, M., and Tanabe, M. (2016). KEGG as a reference resource for gene and protein annotation. Nucleic Acids Res. **44:** D457–D462.

Keilwagen, J., Wenk, M., Erickson, J.L., Schattat, M.H., Grau, J., and Hartung, F. (2016). Using intron position conservation for homology-based gene prediction. Nucleic Acids Res. **44:** e89.

Kim, D., Langmead, B., and Salzberg, S.L. (2015). HISAT: A fast spliced aligner with low memory requirements. Nat. Methods **12:** 357–360.

Komatsuda, T., Pourkheirandish, M., He, C., Azhaguvel, P., Kanamori, H., Perovic, D., Stein, N., Graner, A., Wicker, T., Tagir, A., et al. (2007). Six-rowed barley originated from a mutation in a homeodomain-leucine zipper I-class homeobox gene. Proc. Nat. Acad. Sci. U.S.A. **104:** 1424–1429.

Korf, I. (2004). Gene finding in novel genomes. BMC Bioinform. **5:** 1–9.

Langmead, B., Trapnell, C., Pop, M., and Salzberg, S.L. (2009). Ultrafast and memory-efficient alignment of short DNA sequences to the human genome. Genome Biol. **10:** R25.

Li, D. (1997). The biodiversity and conservation of bamboos in Yunnan, China. The Bamboos **13:** 83–94.

Li, H. (2018). Minimap2: Pairwise alignment for nucleotide sequences. Bioinformatics **34:** 3094–3100.

Li, H., and Durbin, R. (2009). Fast and accurate short read alignment with Burrows–Wheeler transform. Bioinformatics **25:** 1754–1760.

Li, L., Cheng, Z., Ma, Y., Bai, Q., Li, X., Cao, Z., Wu, Z., and Gao, J. (2018). The association of hormone signalling genes, transcription and changes in shoot anatomy during moso bamboo growth. Plant Biotechnol. J. **16:** 72–85.

Li, R., Li, Y., Kristiansen, K., and Wang, J. (2008). SOAP: Short oligonucleotide alignment program. Bioinformatics **24:** 713–714.

Li, R., Zhu, H., Ruan, J., Qian, W., Fang, X., Shi, Z., Li, Y., Li, S., Shan, G., and Kristiansen, K. (2010). *De novo* assembly of human genomes with massively parallel short read sequencing. Genome Res. **20:** 265–272.

Liu, M., Li, W., Wang, H., Zhang, X., and Yu, Y. (2020). The distribution of Furfuryl Alcohol (FA) resin in bamboo materials after surface furfurylation. Materials **13:** 1157.

Lv, Z., Yu, L., Zhan, H., Li, J., Wang, C., Huang, L., and Wang, S. (2023). Shoot differentiation from Dendrocalamus brandisii callus and the related physiological roles of sugar and hormones during shoot differentiation. Tree Physiol. **43:** 1159–1186.

Martins, I.L., Charneira, C., Gandin, V., Ferreira da Silva, J.L., Justino, G.C., Telo, J.P., Vieira, A.J., Marzano, C., and Antunes, A.M. (2015). Selenium-containing chrysin and quercetin derivatives: Attractive scaffolds for cancer therapy. J. Med. Chem. **58:** 4250–4265.

Nawrocki, E.P., and Eddy, S.R. (2013). Infernal 1.1: 100-fold faster RNA homology searches. Bioinformatics **29:** 2933–2935.

Neumann, P., Novák, P., Hoštáková, N., and Macas, J. (2019). Systematic survey of plant LTR-retrotransposons elucidates phylogenetic relationships of their polyprotein domains and provides a reference for element classification. Mob. DNA **10:** 1–17.

Nguyen, L.-T., Schmidt, H.A., Von Haeseler, A., and Minh, B.Q. (2015). IQ-TREE: A fast and effective stochastic algorithm for estimating maximum-likelihood phylogenies. Mol. Biol. Evol. **32:** 268–274.

Nirmala, C., David, E., and Sharma, M. (2007). Changes in nutrient components during ageing of emerging juvenile bamboo shoots. Int. J. Food Sci. Nutr. **58:** 612–618.

Ou, S., Chen, J., and Jiang, N. (2018). Assessing genome assembly quality using the LTR Assembly Index (LAI). Nucleic Acids Res. **46:** e126.

Ou, S., and Jiang, N. (2018). LTR_retriever: A highly accurate and sensitive program for identification of long terminal repeat retrotransposons. Plant Physiol. **176:** 1410–1422.

Pandey, A.K., and Ojha, V. (2013). Standardization of harvesting age of bamboo shoots with respect to nutritional and anti-nutritional components. J. Forestry Res. **24:** 83–90.

Parra, G., Bradnam, K., and Korf, I. (2007). CEGMA: A pipeline to accurately annotate core genes in eukaryotic genomes. Bioinformatics **23:** 1061–1067.

Peng, Z., Lu, Y., Li, L., Zhao, Q., Feng, Q., Gao, Z., Lu, H., Hu, T., Yao, N., Liu, K., et al. (2013). The draft genome of the fast-growing non-timber forest species moso bamboo (Phyllostachys heterocycla). Nat. Genet. **45:** 456–461.

Pertea, M., Pertea, G.M., Antonescu, C.M., Chang, T.-C., Mendell, J.T., and Salzberg, S.L. (2015). StringTie enables improved reconstruction of a transcriptome from RNA-seq reads. Nat. Biotechnol. **33:** 290–295.

Price, A.L., Jones, N.C., and Pevzner, P.A. (2005). De novo identification of repeat families in large genomes. Bioinformatics **21:** i351–i358.

Puttick, M.N. (2019). MCMCtreeR: Fnctions to prepare MCMCtree analyses and visualize posterior ages on trees. Bioinformatics **35:** 5321–5322.

Rice, P., Longden, I., and Bleasby, A. (2000). EMBOSS: The European molecular biology open software suite. Trends Genet. **16:** 276–277.

Robinson, M.D., McCarthy, D.J., and Smyth, G.K. (2010). edgeR: A Bioconductor package for differential expression analysis of digital gene expression data. Bioinformatics **26:** 139–140.

Scurlock, J.M., Dayton, D.C., and Hames, B. (2000). Bamboo: An overlooked biomass resource? Biomass Bioenergy **19:** 229–244.

Seethalakshmi, K., Kumar, M.M., Pillai, K.S., and Sarojam, N. (1998). *Bamboos of India: A compendium* (Brill: Boston, MA, USA).

Servant, N., Varoquaux, N., Lajoie, B.R., Viara, E., Chen, C.J., Vert, J.P., Heard, E., Dekker, J., and Barillot, E. (2015). HiC-Pro: An optimized and flexible pipeline for Hi-C data processing. Genome Biol. **16:** 259.

Simão, F.A., Waterhouse, R.M., Ioannidis, P., Kriventseva, E.V., and Zdobnov, E.M. (2015). BUSCO: Assessing genome assembly and annotation completeness with single-copy orthologs. Bioinformatics **31:** 3210–3212.

Stanke, M., Diekhans, M., Baertsch, R., and Haussler, D. (2008). Using native and syntenically mapped cDNA alignments to improve de novo gene finding. Bioinformatics **24:** 637–644.

Sun, J., Ding, Z.-Q., Gao, Q., Xun, H., Tang, F., and Xia, E.-D. (2016). Major chemical constituents of bamboo shoots (*Phyllostachys pubescens*): Qualitative and quantitative research. J. Agri. Food Chem. **64:** 2498–2505.

Tang, S., Lomsadze, A., and Borodovsky, M. (2015). Identification of protein coding regions in RNA transcripts. Nucleic Acids Res. **43:** e78.

Teng, J., Xiang, T., Huang, Z., Wu, J., Jiang, P., Meng, C., Li, Y., and Fuhrmann, J.J. (2016). Spatial distribution and variability of carbon storage in different sympodial bamboo species in China. J. Environ. Manage. **168:** 46–52.

Trincado, J.L., Entizne, J.C., Hysenaj, G., Singh, B., Skalic, M., Elliott, D.J., and Eyras, E. (2018). SUPPA2: Fast, accurate, and uncertainty-aware differential splicing analysis across multiple conditions. Genome Biol. **19:** 40.

User, G.B.O. (2023). *Occurrence download*. (GBIF: Copenhagen, Denmark).

Venkatachalam, P., Kalaiarasi, K., and Sreeramanan, S. (2015). Influence of plant growth regulators (PGRs) and various additives on in vitro plant propagation of Bambusa arundinacea (Retz.) Wild: A recalcitrant bamboo species. J. Genet. Eng. Biotechnol. **13:** 193–200.

Vurture, G.W., Sedlazeck, F.J., Nattestad, M., Underwood, C.J., Fang, H., Gurtowski, J., and Schatz, M.C. (2017). GenomeScope: Fast reference-free genome profiling from short reads. Bioinformatics **33:** 2202–2204.

Wang, K., Peng, H., Lin, E., Jin, Q., Hua, X., Yao, S., Bian, H., Han, N., Pan, J., Wang, J., et al. (2010). Identification of genes related to the development of bamboo rhizome bud. J. Exp. Bot. **61:** 551–561.

Wei, Q., Guo, L., Jiao, C., Fei, Z., Chen, M., Cao, J., Ding, Y., and Yuan, Q. (2019). Characterization of the developmental dynamics of the elongation of a bamboo internode during the fast growth stage. Tree Physiol. **39:** 1201–1214.

Wheeler, T.J., Clements, J., Eddy, S.R., Hubley, R., Jones, T.A., Jurka, J., Smit, A.F., and Finn, R.D. (2012). Dfam: A database of repetitive DNA based on profile hidden Markov models. Nucleic Acids Res. **41:** D70–D82.

Xu, Z., and Wang, H. (2007). LTR_FINDER: An efficient tool for the prediction of full-length LTR retrotransposons. Nucleic Acids Res. **35:** W265–W268.

Yang, J.B., Dong, Y.R., Wong, K.M., Gu, Z.J., Yang, H.Q., and Li, Z. (2018). Genetic structure and differentiation in Dendrocalamus sinicus (Poaceae: Bambusoideae) populations provide insight into evolutionary history and speciation of woody bamboos. Sci. Rep. **8:** 16933.

Yang, Z. (1997). PAML: A program package for phylogenetic analysis by maximum likelihood. Computer App. Biosci. **13:** 555–556.

Zhan, H., Zhang, L.-y., Deng, L., Niu, Z.-h., Li, M.-b., Wang, C.-m., and Wang, S. (2018). Physiological and anatomical response of foliar silicon application to Dendrocalamus brandisii plantlet leaves under chilling. Acta Physiol. Plant. **40:** 1–14.

Zhang, T., and Wan, J. (2004). The organizationl culture and quick proliferate propation of Dendrocalamus brandisi. J. Yunnan Minzu Univ. Nat. Sci. Ed. **13:** 203–206.

Zhao, H., Gao, Z., Wang, L., Wang, J., Wang, S., Fei, B., Chen, C., Shi, C., Liu, X., Zhang, H., et al. (2018). Chromosome-level reference genome and alternative splicing atlas of moso bamboo (*Phyllostachys edulis*). Gigascience **7:** giy115.

Zheng, Y., Yang, D., Rong, J., Chen, L., Zhu, Q., He, T., Chen, L., Ye, J., Fan, L., Gao, Y., et al. (2022). Allele-aware chromosome-scale assembly of the allopolyploid genome of hexaploid Ma bamboo (*Dendrocalamus latiflorus* Munro). J. Integr. Plant. Biol. **64:** 649–670.

Zhong, Y., Chen, W., and Tan, H. (2019). A study of tissue culture and seedling transplanting technology for dendrocalamus brandiss. World Bamboo Rattan **17:** 31–35.

Zwaenepoel, A., and Van de Peer, Y. (2019). wgd—Simple command line tools for the analysis of ancient whole-genome duplications. Bioinformatics **35:** 2153–2155.

SUPPORTING INFORMATION

Additional Supporting Information may be found online in the supporting information tab for this article: http://onlinelibrary.wiley.com/doi/10.1111/jipb.13592/suppinfo

Figure S1. Genome survey based on a frequency distribution map

Figure S2. Collinearity relationships of *Dendrocalamus brandisii* with three Gramineae species

Figure S3. Gene Ontology (GO) terms and Kyoto Encyclopedia of Genes and Genomes (KEGG) pathway enrichment analyses for gene families in *Dendrocalamus brandisii*

Figure S4. Gene Ontology (GO) terms and Kyoto Encyclopedia of Genes and Genomes (KEGG) pathway enrichment analyses for contracted gene families in *Dendrocalamus brandisii*

Figure S5. Gene Ontology (GO) terms and Kyoto Encyclopedia of Genes and Genomes (KEGG) pathway enrichment analyses for expanded gene families in *Dendrocalamus brandisii*

Figure S6. Gene Ontology (GO) term enrichment analysis for alternative polyadenylation (APA) genes in *Dendrocalamus brandisii*

Figure S7. Export and import trade of bamboo shoots in different countries

Table S1. The distribution coordinates of *Dendrocalamus* around the world

Table S2. The distribution coordinates of *Dendrocalamus brandisii* around the world